Pore pressure evolution in deforming granular material: A general formulation and the infinitely stiff approximation

L. Goren,[1] E. Aharonov,[2] D. Sparks,[3] and R. Toussaint[4]

Received 7 December 2009; revised 20 April 2010; accepted 29 April 2010; published 30 September 2010.

[1] The physics of deformation of fluid-filled granular media controls many geophysical systems, ranging from shear on geological faults to landslides and soil liquefaction. Its great complexity is rooted in the mechanical coupling between two deforming phases: the solid granular network and the fluid-filled pore network. Often deformation of the granular network leads to pore fluid pressure (PP) changes. If the PP rises enough, the fluid-filled granular media may transition from a stress-supporting grain network to a flowing grain-fluid slurry, with an accompanying catastrophic loss of shear strength. Despite its great importance, the mechanisms and parameters controlling PP evolution by granular shear are not well understood. A formulation describing the general physics of pore fluid response to granular media deformation is developed and used to study simple scenarios that lead to PP changes. We focus on the infinitely stiff end-member scenario, where granular deformation is prescribed, and the PP responds to this deformation. This end-member scenario illustrates the two possible modes of pore fluid pressurization: (1) via rapid fluid flow when fluid drainage is good and (2) via pore volume compaction when drainage is poor. In the former case the rate of deformation controls PP evolution, while in the latter case, fluid compressibility is found to be an important parameter and the amount of pressurization is controlled by the overall compaction. The newly suggested fluid-induced mechanism (mechanism 1) may help explain observations of liquefaction of initially compact soils and shear zones.

Citation: Goren, L., E. Aharonov, D. Sparks, and R. Toussaint (2010), Pore pressure evolution in deforming granular material: A general formulation and the infinitely stiff approximation, *J. Geophys. Res.*, *115*, B09216, doi:10.1029/2009JB007191.

1. Introduction

[2] Soils, unconsolidated rocks, and fault gouge may be described as porous skeletons composed of contacting grains. Often the pores are filled with fluid. The grains and the fluid form two intertwined networks: the grains connect via frictional contacts forming a heterogeneous deformable solid network, while the fluid flows in the complementary network of pores. The coupled solid-fluid system may deform in response to applied stresses, and deformation naturally arises on all timescales: from slow compaction in response to sediment load, to catastrophic failure during earthquakes and landslides. The granular network may deform elastically or through irreversible rearrangements (e.g., pore collapse). Such deformation changes the pore volume and by that affects the pore fluid pressure (PP). On the other hand, gradients in PP exert forces that may cause grains to move and the solid network to deform. The coupling between the solid matrix deformation and the value of PP is possibly the most important aspect of solid-fluid coupling: elevated PP modifies the way in which saturated granular soils and rocks respond to stresses, and often controls devastating natural phenomena such as earthquakes [e.g., *Sleep and Blanpied*, 1992], landslides [e.g., *Voight and Faust*, 1982; *Iverson et al.*, 1997] and soil liquefaction [*Das*, 1993; *Kramer*, 1996]. A continuum view of how PP modifies the system response to stress is formulated in the law of effective stress [*Terzaghi*, 1943]. The most important aspect of this law is the fact that the shear resistance, τ, of saturated granular material decreases linearly with increasing PP, P, since $\tau \propto \sigma - P$, where σ is the confining stress [*Terzaghi*, 1943; *Scholz*, 1990]. Therefore, the ability of saturated soils to resist shear is crucially dependent on the state of their PP: under normal conditions, when $P < \sigma$, grain-networks behave like solids that can sustain shear stresses. However, if for some reason the PP is elevated to a level where $P = \sigma$ the shear resistance vanishes, and 'liquefaction' occurs, a situation in which the grain-fluid system flows like a fluid in response to even small shear stresses. When PP within a landslide shear zone approaches the confining stress, the slide may accelerate catastrophically. When fault gouge material experiences high

[1]Department of Environmental Sciences and Energy Research, Weizmann Institute of Science, Rehovot, Israel.
[2]Institute of Earth Sciences, Hebrew University, Jerusalem, Israel.
[3]Department of Geology and Geophysics, Texas A&M University, College Station, Texas, USA.
[4]IPGS, CNRS and University of Strasbourg, EOST, Strasbourg, France.

0148-0227/10/2009JB007191

values of PP, the dramatic reduction of shear resistance may lead to dynamic acceleration and an earthquake in response to background tectonic stresses that were previously sustained by the fault resistance to sliding. In soils, an increase in PP leading to liquefaction may cause collapse of previously supported infrastructure.

[3] Traditionally, the mechanics of fluid-filled soils, landslides' shear zone and gouge material are studied separately. Indeed, a major difference between these three systems is their characteristic depth. While soil liquefaction is a phenomenon of the very shallow crust and is usually restricted to few tens of meters below the surface, the depth of landslides' shear zones ranges between several meters to few kilometers [e.g., *Sidle and Ochiai*, 2006], and the depth of fault gouge is restricted to the seismogenic zone, normally 2–30 km. The different depths result in differences in the effective confining stresses. This range of depth is also accompanied by a range of drainage conditions [*Saar and Manga*, 2004].

[4] Despite depth and drainage differences, the basic coupled mechanics of grains and fluid may be applied similarly to soils, shear zones, and gouge layers. Indeed, it will be shown here that the formulation of pore fluid response to granular matrix deformation is depth independent. For that reason, conclusions from various studies (some of them reviewed in Appendix A) that deal with pore fluid pressurization for one system may be applied also to the other systems. Therefore the term 'liquefaction' is used here to address the general case of PP equals the confining stress, regardless of the geological setting (soil, landslides' shear zone, and gouge layers). Caution should be practiced when interpreting the results, as the PP required to liquefy soils is smaller by orders of magnitude than that required to completely liquefy gouge layers. In the rest of the introduction, the importance of PP to soil liquefaction and pressurization along gouge layers is reviewed separately, but the mechanics controlling PP evolution is presented and discussed uniformly.

[5] Soil liquefaction [*Das*, 1993; *Kramer*, 1996] is triggered by and contributes to the devastation of earthquakes, and may cause collapse of infrastructure foundations, and initiate landslides. In the process of soil liquefaction, seismic waves induce cyclic loading, which causes the PP to rise. As a consequence, the granular system, which under normal conditions behaves like a solid that resists shear, loses its shear resistance and may flow as a fluid. As a result, liquefied soil can no longer support the infrastructure that is rooted in it and a catastrophic collapse of buildings, roads, bridges and other structures with foundations may take place (e.g., damage during earthquakes at Niigata, 1964 [*Kawakami and Asada*, 1966], or Izmit, 1999 [*Cetin et al.*, 2004]). In some earthquakes, the damage caused by liquefaction exceeds the damage by direct ground acceleration. For example, the 1995 earthquake in Kobe, Japan, caused liquefaction that resulted in more than 5500 deaths, and an estimated economic loss of over $US 130 billion [*Scawthorn and Yanev*, 1995].

[6] Since liquefaction models are a practical necessity in geotechnical engineering, phenomenological models of coupled solid-fluid deformation have been developed (for a review, see *Sawicki and Mierczynski* [2006]). These models are usually based on continuum mixture theory formulations, and use experimental data for model calibration. A major effort to determine the mechanisms involved in earthquake-induced soil liquefaction by comparing centrifuge experiment with phenomenological numerical models took place as part of the VELACS project [*Popescu and Prevost*, 1995]. None of the models accurately predict the set of experimental outcomes and by themselves show a wide and inconsistent range of predictions [*Manzari et al.*, 1994]. Recently, more sophisticated phenomenological models have improved the predictability of PP buildup and dissipation [*Zienkiewicz et al.*, 1999].

[7] Catastrophic pore fluid pressurization may occur not only in response to cyclic loading induced by earthquakes, but also as a result of continuous shearing of fluid-filled granular layers. This is the most studied scenario for liquefaction within shear zones of landslides and gouge-filled faults. In these cases, drainage conditions and porosity evolution were shown to control PP evolution and thus layer strength. Dynamic dilation and compaction of gouge and shear zone material are shown to be a function of shearing velocity [*Marone et al.*, 1990] and stress conditions [*Iverson et al.*, 2000; *Aharonov and Sparks*, 2002]. When the fault is sealed dilation often leads to stable sliding as it causes PP reduction and fault hardening [*Scholz*, 1990; *Segall and Rice*, 1995; *Moore and Iverson*, 2002], while shear-enhanced compaction of under-compacted gouge may lead to extreme weakening and unstable sliding [*Blanpied et al.*, 1992]. Pore fluid pressurization and migration also control communication between fault zones and earthquakes sequencing [*Yamashita*, 1999; *Miller and Nur*, 2000].

[8] In terms of the physics of the granular-fluid system, a matrix of granular media may deform elastically through small reversible deformation at grain contacts, and/or plastically through irreversible rearrangements (e.g., pore collapse). The term poroplasticity [*Kherbouche et al.*, 1995] is used here to describe such irreversible deformation of granular media in a way that modifies the shape and size of pores and the contact network between grains, and is unrelated to microscopic dislocation glide; that is, rearrangements take place by grains sliding and rolling relative to each other, and thus change the matrix configuration. The traditional approach suggests that poroplasticity may lead to fluid pressurization and may cause liquefaction [*Sawicki and Mierczynski*, 2006]. More recently a different view on the mechanics of liquefaction was suggested: poroelasticity was offered to be the possible cause of liquefaction induced by earthquakes [*Bachrach et al.*, 2001]. Sections 1.1 and 1.2 briefly review poroplastic and poroelastic approaches and demonstrate that the physical understanding of the mechanisms by which matrix deformation generates large enough PP for soils and gouge layers to liquefy is not complete. The rheological regime that controls PP evolution, poroplasticity or poroelasticity, is still debated and so are the relevant boundary conditions (drained and undrained), and the importance of physical parameters such as fluid compressibility.

1.1. Poroplastic Path to Liquefaction: Current State of Understanding

[9] The poroplastic view of liquefaction relates the generation of high PP to irreversible collapse of pore volume

under undrained conditions [*Sawicki and Mierczynski*, 2006]. This mechanism is supported by laboratory experiments showing that when loose sediments compact under cyclic shear [*Casagrande*, 1936; *Youd*, 1972], PP rises under undrained conditions [*Castro*, 1969]. Many models of poroplastic deformation assume specific deformation laws of the porous configuration: in the context of soil liquefaction with matrix compaction induced by mechanical vibrations [*Snieder and van der Beukel*, 2004], in relation to crustal processes with material precipitation within pores [*Walder and Nur*, 1984], and in the context of gouge material with porosity that depends on slip [*Yamashita*, 1999] and slip velocity [*Segall and Rice*, 1995; *Samuelson et al.*, 2009].

[10] Recently, fully coupled grain-scale models of grains and pore fluid were developed to study the relation between general deformation of a granular matrix and soil liquefaction [e.g., *El Shamy and Zeghal*, 2007; *Okada and Ochiai*,2007; *Li et al.*, 2007]. Such models use the discrete element method and are capable of simulating both poroelastic and poroplastic grain rearrangements. Here we review two of these studies that demonstrate the inconsistency in the assumed physics of soil liquefaction: (1) *El Shamy and Zeghal* [2007] study a drained system (where the fluid is allowed to flow freely out of the top boundary) with forcing induced by cyclic shear acceleration at the base of the system and assume that pore fluid is completely incompressible, an assumption that follows many engineering interpretation of experiments [e.g., *Garga and Zhang*, 1997; *Kozlov et al.*, 1998]. (2) *Okada and Ochiai* [2007] study an undrained system (with impermeable boundaries) placed under contractive strain, and assume a compressible pore fluid. Both studies report the generation of high enough PP for liquefaction to occur, while the latter study emphasizes that high PP was generated only in initially loosely packed systems. Thus, these two works study the same problem but assume different physics (incompressible versus compressible fluid) and different boundary conditions (drained versus undrained). The results of *Okada and Ochiai* [2007] can be interpreted within the classical framework of soil liquefaction, as they observe high PP when compacting a loosely packed undrained granular system. However, the results of *El Shamy and Zeghal* [2007] are somewhat unexpected because they observe liquefaction under drained conditions with incompressible fluid. Indeed, a similar model that is described by *Itasca Consulting Group Inc.* [2005], stresses that liquefaction cannot be simulated with an incompressible fluid because then the model "does not include a mechanism for generation of pore pressure under strain." In section 6 we supply a physical explanation for this apparent violation of the classical view of liquefaction and show that the two models of *El Shamy and Zeghal* [2007] and *Okada and Ochiai* [2007] represent different end-members of the same physical system.

1.2. Poroelastic Path to Liquefaction: Current State of Understanding

[11] Poroelastic theory for coupled solid-fluid deformation [*Terzaghi*, 1943; *Biot*, 1941, 1956a, 1956b, 1962; *Skempton*, 1960; *Wang*, 2000] assumes infinitely small reversible deformations, (an assumption better suited for rocks and cohesive matter than for granular media) and calculates solid deformation and PP. The poroelastic view attributes PP variations to the coupling between the elastic deformation of pores and the porous flow induced by the passage of P-waves [*Bachrach et al.*, 2001]. A Biot based model is developed by *Bachrach et al.* [2001], which shows that compressible fluid and low shear modulus of the granular matrix may lead to PP that exceeds the loading. A similar formulation, but without inertial terms, is developed by *Wang* [2000] for the general study of PP response to cyclic loading from a poroelastic point of view. Section 3 shows that PP rise using this mechanism may lead to soil liquefaction only in the very top of the sediment column, and to gouge liquefaction only if the fluid was initially highly pressurized.

1.3. Overview

[12] The diversity of models and approaches and the ongoing debates regarding the basic physics of liquefaction indicate that a coherent physical theory that explains how PP evolves in response to general deformation of the granular matrix is still missing. Such a unifying theory should be able to explain as particular cases the various field, experimental and numerical observations and the links between existing models. It should also address some basic questions that were left unanswered: What is the role of fluid compressibility [*Garga and Zhang*, 1997]? Can liquefaction take place under drained conditions [*Das*, 1993]? And how does liquefaction occur in initially over-compacted soils [*Soga*, 1998]?

[13] The work presented here aims to do exactly that. In order to achieve this goal, we first develop a general theory and then apply it within the scope of the infinite stiffness approximation, where the granular deformation is prescribed and the pore fluid responds to this deformation, without affecting solid matrix deformation. The study of this simple end-member case allows derivation of analytical solutions for the mechanics of pore fluid pressurization, and comparison to numerical solutions. The behavior of this end-member situation is simple but yet rich enough to highlight the mechanisms that control liquefaction.

[14] In this paper we develop a mass and momentum conservation based formulation for the general PP response to granular matrix deformation in section 2. This formulation is not restricted to a particular type of deformation and may be used to study both elastic reversible processes and irreversible plastic deformation. The question of poroelastic versus poroplastic rheology is discussed in section 3. Then, to study pore fluid behavior under the infinite stiffness approximation, section 4 describes the application of the formulation to a simple system of uniform grains immersed in fluid and subjected to shear loading. Section 5 analyzes the equation that lies at the heart of the pore fluid formulation, and reveals different physical processes that control the evolution of PP. One of these processes may explain liquefaction events in initially over-consolidated granular material under drained conditions. Analysis and implications are discussed in section 6, and we present our conclusions in section 7. In Appendix A we show that our formulation for the pore fluid pressure is a generalization of previous models and thus we can uncover the missing links between them. In

Appendix B we develop a general analytic solution for the basic equation that describes pore fluid pressurization.

2. Theoretical Model

[15] In this section, mass and momentum conservation laws are used for the development of an equation describing the spatial and temporal evolution of excess pore fluid pressure in response to granular or porous matrix deformation. Let Φ be the porosity, t the time, ρ_s and ρ_f the mass densities of the bulk material of the grains and of the fluid, respectively, and $\mathbf{u_s}$ and $\mathbf{u_f}$ the grains and fluid velocities, respectively. The velocities are considered at a representative scale for Darcy's law; that is, they are defined for mesoscopic volumes containing at least a few grains. First, mass conservation equations are written for the grains and for the fluid:

$$\frac{\partial[(1-\Phi)\rho_s]}{\partial t} + \nabla\cdot[(1-\Phi)\rho_s\mathbf{u_s}] = 0, \tag{1}$$

$$\frac{\partial[\Phi\rho_f]}{\partial t} + \nabla\cdot[\Phi\rho_f\mathbf{u_f}] = 0, \tag{2}$$

where $\nabla\cdot$ is a divergence operator related to grains/fluid advective processes. The quantity $\Phi(\mathbf{u_f}-\mathbf{u_s})$ corresponds to the Darcy velocity [*Anghel et al.*, 2006], i.e.,

$$\Phi(\mathbf{u_f}-\mathbf{u_s}) = -\frac{k}{\mu}\nabla P, \tag{3}$$

where k is the permeability, μ is the fluid viscosity and P is the excess (over hydrostatic) fluid pressure. Equation (3), Darcy's law, is derived from Stoke's equation, and is a reduced form of the momentum equation under the assumption of negligible fluid inertia. The fluid density is given by the fluid state equation:

$$\rho_f = \rho_0(1+\beta P), \tag{4}$$

where ρ_0 is the fluid density at a reference hydrostatic pressure level, and β is the adiabatic fluid compressibility, $\beta = (1/\rho_f)(\partial\rho_f/\partial P)$. Using the adiabatic compressibility means assuming no significant heat exchange between the overpressured and underpressured zones during fast motion. We assume that grain compressibility is negligible relative to the fluid compressibility, as expected for natural sand filled with fluid such as water, so that ρ_s can be approximated as constant, and equations (1) to (4) lead to

$$\beta\Phi\frac{\partial P}{\partial t} = \nabla\cdot\left[(1+\beta P)\frac{k}{\mu}\nabla P\right] - (1+\beta P)\nabla\cdot\mathbf{u_s} - \beta\Phi\mathbf{u_s}\cdot\nabla P. \tag{5}$$

This derivation is based on the same basic principles as the approach used successfully to model instabilities in the flow of granular media and fluids [*Vinningland et al.*, 2007a, 2007b; *Johnsen et al.*, 2006, 2007, 2008], and hydrofracture [*Flekkøy et al.*, 2002]. The value of the excess PP, P, has, for the cases considered, an upper bound set approximately by the difference between the lithostatic and hydrostatic stresses, $\sigma_d = (\rho_s - \rho_f)gh$, where h is the depth at which matrix deformation occurs. Indeed, when $P = \sigma_d$ the effective stress vanishes, and liquefaction may occur. For that reason the analysis presented here considers the case of

$$\beta P \le \beta\sigma_d \ll 1. \tag{6}$$

Taking fluid compressibility of $\beta = 4.5\times10^{-10}$ Pa^{-1} [*Garga and Zhang*, 1997, and references therein], equation (6) bounds $\sigma_d \ll 2.22$ GPa and $h \ll 150$ km. This restriction on h does not limit the analysis since soil liquefaction is a phenomenon of the shallow crust, and fault gouge material is restricted by the base of the seismogenic zone. It should be noted that here we consider a single fluid with low compressibility, such as water, in the pore space. If the pore space is filled with water/air mixture, the mixture compressibility is expected to increase significantly with respect to pure water and equation (6) might not hold. This situation is not considered in the present paper. Following (6), equation (5) is rewritten as

$$\beta\Phi\frac{\partial P}{\partial t} = \nabla\cdot\left[\frac{k}{\mu}\nabla P\right] - \nabla\cdot\mathbf{u_s} - \beta\Phi\mathbf{u_s}\cdot\nabla P. \tag{7}$$

The first and fourth term of equation (7) compose together the Lagrangian derivative of the PP, the second term describes PP diffusion and the third term may be viewed as the forcing, due to spatial differences in grain velocities.

[16] To investigate the relative magnitude of the different terms in equation (7), a non-dimensional analysis is performed. Let us define the characteristic magnitude of the variables in the model: $P = \hat{P}/\beta$, $\mathbf{u_s} = \hat{\mathbf{u}}_\mathbf{s}u_0$, $k = \hat{k}k_0$, and $t = \hat{t}t_0$, where the $\hat{}$ notation denotes non-dimensional variables, and u_0, k_0, and t_0 are the velocity, permeability, and timescale factors, respectively. The divergence arising from equations (1) and (2) represents grain-scale rearrangements. Therefore, the derivatives in these operators are scaled by d^{-1}, a characteristic grain diameter, and $\nabla\cdot = \hat{\nabla}_1\cdot/d$. However, the gradient operator in equation (3) represents a larger length scale, over which Darcy law applies. Therefore the derivatives in this operator are scaled by l_k^{-1}, the PP diffusion length scale, and $\nabla = \hat{\nabla}_2/l_k$. l_k is bounded from the top by h, and is presumably much larger than d. A natural choice for l_k is $\sqrt{Dt_0}$, where $D = k_0/\beta\mu\Phi$ is the PP diffusion coefficient, and $t_0 = d/u_0$ is the timescale of deformation. Assigning the non-dimensional variables in equation (7) results in

$$\frac{\partial\hat{P}}{\partial\hat{t}} = \frac{D}{l_k u_0}\hat{\nabla}_1\cdot(\hat{k}\hat{\nabla}_2\hat{P}) - \frac{1}{\Phi}\hat{\nabla}_1\cdot\hat{\mathbf{u}}_\mathbf{s} - \frac{d}{l_k}\hat{\mathbf{u}}_\mathbf{s}\cdot\hat{\nabla}_2\hat{P}. \tag{8}$$

[17] In equation (8), the coefficients of both the second and the fourth terms may be expressed as functions of either a Peclet number, or a Deborah number, which are identical to each other: $D/l_k u_0 = \sqrt{\mathrm{Pe}^{-1}} = \sqrt{\mathrm{De}_d^{-1}}$, and $d/l_k = \sqrt{\mathrm{Pe}} = \sqrt{\mathrm{De}_d}$. The Peclet number, $\mathrm{Pe} = du_0/D$, expresses the ratio between the rate of advection, u_0, and the rate of PP diffusion across a single grain, D/d [*McNamara et al.*, 2000]. The Deborah number, $\mathrm{De}_d = t_d/t_0$, is defined as the ratio of relaxation timescale and a characteristic process timescale [*Osswald*, 1998, p. 54]. Here, the relaxation timescale, $t_d = d^2/D$, is the timescale for PP diffusion across a single grain,

and the characteristic process timescale, t_0, is the timescale of deformation.

[18] In the following, we use the Deborah number notation, De_d, where subscript d is added because later in this paper an additional relaxation timescale will be considered. De_d is termed the grain Deborah number. There are two limits to equation (8), one when $\mathrm{De}_d \gg 1$, and then the second diffusion term in equation (8) is negligible, and one when $\mathrm{De}_d \ll 1$, and then the last term in equation (8) is negligible. The case of $\mathrm{De}_d > 1$ is an unnatural end-member. Assuming pore fluid water, Carman-Kozeny permeability ($k \propto d^2$), and deformation rate <10 m/s, this end-member occurs only if grain size in unrealistically small (the order of 100 nm). In fact, for most natural cases, and in particular for the cases considered in this paper, $\mathrm{De}_d \ll 1$. As a result, the fourth term (the gradient part of the Lagrangian derivative) in equation (8) may be neglected. Equation (8) may then be rewritten as

$$\frac{\partial \hat{P}}{\partial \hat{t}} = \sqrt{\mathrm{De}_d^{-1}}\hat{\nabla}_1 \cdot (\hat{k}\hat{\nabla}_2\hat{P}) - \frac{1}{\Phi}\hat{\nabla}_1 \cdot \hat{\mathbf{u}}_\mathbf{s}, \tag{9}$$

where only three terms are left. In a dimensional form, equation (9) reads

$$\frac{\partial P}{\partial t} = \frac{1}{\beta\Phi\mu}\nabla \cdot [k\nabla P] - \frac{1}{\beta\Phi}\nabla \cdot \mathbf{u}_\mathbf{s}. \tag{10}$$

[19] Such a non-dimensional analysis is not commonly performed in engineering applications of soil liquefaction. Instead, the first time dependent term in equation (10) is normally neglected due to the small value of fluid compressibility, β [e.g., *Garga and Zhang*, 1997; *Kozlov et al.*, 1998]. However, a simple thought experiment can demonstrate its importance: Consider a sealed system, with initially uniform pressure, that is loaded uniformly. The diffusive term in equation (10) is thus zero. If the time dependent term would have been neglected, then equation (10) would reduce to $\nabla \cdot \mathbf{u}_\mathbf{s} = 0$; that is, no deformation could take place due to fluid resistivity to both flow and compression.

[20] The form of the forcing term in equation (10) is intuitive in the framework of poroplasticity: when a fluid-filled granular system compacts and pore volume collapses, $\nabla \cdot \mathbf{u}_\mathbf{s} < 0$, and the PP is expected to rise. When the system dilates, $\nabla \cdot \mathbf{u}_\mathbf{s} > 0$, and the PP will drop. Furthermore, the form of the forcing as dependent on the local grain velocities suits a straightforward plugging of equation (10) in a model of coupled grains and fluid implemented with discrete elements method of the form of *Okada and Ochiai* [2007].

[21] It is sometimes convenient to express the forcing term as a function of the porosity evolution rather than the divergence of the solid grains velocity. From grain mass conservation, equation (1):

$$(1-\Phi)\nabla \cdot \mathbf{u}_\mathbf{s} = \frac{\partial \Phi}{\partial t} + \mathbf{u}_\mathbf{s} \cdot \nabla\Phi. \tag{11}$$

When the initial porosity and the rate of porosity evolution are assumed uniform [e.g., *Walder and Nur*, 1984; *Snieder and van der Beukel*, 2004] $\mathbf{u}_\mathbf{s} \cdot \nabla\Phi = 0$ and $(1-\Phi)\nabla \cdot \mathbf{u}_\mathbf{s} = \partial\Phi/\partial t$. Under these restrictions equation (10) may be rewritten as

$$\frac{\partial P}{\partial t} = \frac{1}{\beta\Phi\mu}\nabla \cdot [k\nabla P] - \frac{1}{\beta\Phi(1-\Phi)}\frac{\partial \Phi}{\partial t}. \tag{12}$$

[22] Formulations similar to our equations (10) or (12) arise in other works dealing with the response of PP to specific situations of granular and porous matrix deformation [*Walder and Nur*, 1984; *Wang*, 2000; *Samuelson et al.*, 2009], some of them specifically in the context of soil liquefaction [*Bachrach et al.*, 2001; *Snieder and van der Beukel*, 2004]. Appendix A demonstrates how these models may be directly compared to our formulation.

3. Poroelastic Pore Fluid Pressurization and Liquefaction

[23] As the formulation presented here is not restricted to a specific rheology (poroelastic or poroplastic), the possibility of generating high PP with a poroelastic mechanism is next examined. For that, we revisit a formulation developed by *Wang* [2000] describing one-dimensional spatiotemporal evolution of PP in response to temporal stressing of a fluid-filled porous material [*Wang*, 2000, equations 3.65 and 6.14]:

$$\frac{\partial P}{\partial t} = \frac{k}{\mu S}\frac{\partial^2 P}{\partial z^2} - \gamma\frac{\partial \sigma_{zz}}{\partial t}, \tag{13}$$

where S is the uniaxial specific storage in Pa^{-1}, γ is the dimensionless loading efficiency, and σ_{zz} is the external elastic loading stress in Pa. $k/\mu S$ is a space and time constant diffusion coefficient, and $\gamma\partial\sigma_{zz}/\partial t$ is the forcing term. Appendix A shows that equation (13) is equivalent to our equation (10) when we assume that $\nabla \cdot \mathbf{u}_\mathbf{s}$ occurs by elastic deformation only, and also demonstrates the equivalency between equation (13) and the formulation of *Bachrach et al.* [2001] under the assumption of negligible inertia. Thus, any conclusion drawn from the analysis in this section applies also to the formulation discussed in section 2. Equation (13) is most suitable for investigating the poroelastic liquefaction hypothesis because its forcing term is given in the form of time dependent elastic stress loading, such as a seismic pressure wave. Indeed, *Wang* [2000] studied the response of equation (13) to loading by stress wave.

[24] *Wang* [2000] solved analytically equation (13) in a half-space, with a forcing, σ_{zz}, of the form

$$\sigma_{zz}(0,t) = -\sigma_0 \exp(i\omega t) \tag{14}$$

where σ_0 is the amplitude of the pressure wave and ω is the loading frequency. The top of the domain is taken as drained and hence $P(z = 0, t) = 0$. Figure 1 shows the resultant PP magnitude, $|P|$, scaled by $\gamma\sigma_0$, as a function of the scaled depth, z/l_k. Note that the maximum value of the loading efficiency, γ, is 1. This maximum value corresponds to the case of low shear modulus for which *Bachrach et al.* [2001] find the maximum value of PP. Figure 1 and *Wang*'s [2000] analysis indicate that when the loading efficiency is maximal, the maximum value of PP obtained in a fluid-filled poroelastic medium when a seismic P-wave passes is

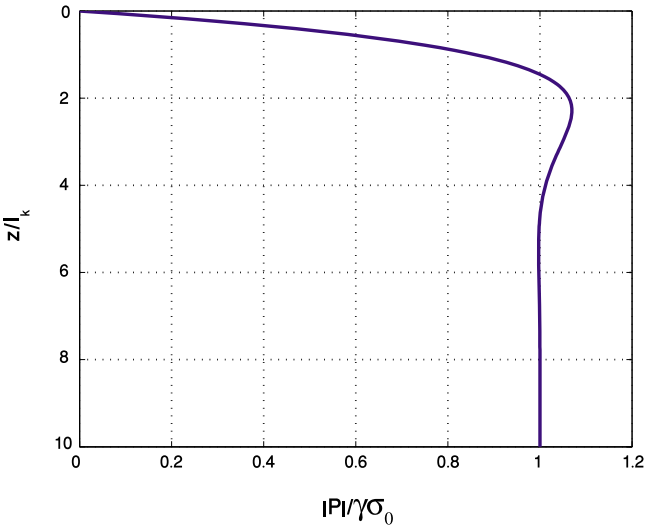

Figure 1. Half-space solution of system of equations (13) and (14), describing the spatial evolution of PP in a poroelastic material under periodic stress loading and drained top. Maximum magnitude of PP, $|P|$, is plotted as a function of normalized depth. $|P|$ is bounded by $1.07\gamma\sigma_0$, where $\gamma \leq 1$ is the loading efficiency and σ_0 is the amplitude of the pressure wave forcing. The relation between $|P|$ and σ_0 indicates that a poroelastic mechanism for liquefaction (see text) is limited to the very top of the soil column. Adopted from *Wang* [2000, Figure 6.11], with permission from Princeton University Press.

bounded by $1.07\sigma_0$. That is, the PP cannot exceed the stress wave amplitude by more than 7%.

[25] For liquefaction to occur, PP must reach lithostatic values [*Sawicki and Mierczynski*, 2006]. If we consider a saturated soil column with a thickness of 1 m, the lithostatic pressure at its base is about 25 kPa, while the hydrostatic pressure is 10 kPa. Therefore there is a need to generate excess of $P = 15$ kPa for liquefaction to occur at a depth of 1m. For the poroelastic liquefaction to occur, the forcing magnitude then must be 14 kPa, two orders of magnitude larger than typical amplitudes of seismic pressure waves [*Bachrach et al.*, 2001]. If we consider a fault gouge at depth of 15 km, the excess PP needed for complete liquefaction is about 0.2 GPa. The excess PP generated by the poroelastic mechanism with a forcing wave of 100 Pa is a negligible fraction of the needed value. These simple examples indicate that the poroelastic path to liquefaction is applicable only for the top few centimeters of the grains-fluid column, or when PP is initially very close to lithostatic values. Therefore, in section 4 we turn back to study the classical poroplastic volume collapse mechanism using a simple prescribed plastic matrix deformation model.

4. Infinite Stiffness Approximation

[26] The formulation presented so far is applicable to a general fully coupled system. But in order to actually solve the fully coupled grain-fluid deformation, another equation for the evolution of solid grain momentum should be prescribed. In this equation, PP gradients exert forces on the granular matrix [e.g., *McNamara et al.*, 2000], sometimes referred to as seepage forces [*Mourgues and Cobbold*, 2003; *Rozhko et al.*, 2007]. However, here we first solve a simpler scenario, the infinitely stiff system, which means that the matrix deformation is externally prescribed and the PP only responds to this deformation. The reason we do not immediately solve also the other direction (that of the deformation of the solid matrix in response to PP gradients), is twofold: First, because currently there is no first principles based theory that predicts the general (elastic and plastic) granular matrix deformation induced by a PP field that varies spatially and temporally. Moreover, currently there is not even a first principles based theory that predicts the deformational response of a dry granular matrix to general loading [*Forterre and Pouliquen*, 2008]. To overcome this limitation, previous works that solve for the fully coupled system with a continuum approach use phenomenological relations to describe the porosity evolution in response to external loading and PP variations [e.g., *Snieder and van der Beukel*, 2004; *Samuelson et al.*, 2009] and in rocks [*Hamiel et al.*, 2005]. Consequently, they are restricted to a specific type of deformation, material properties, and boundary conditions. A second possible method to obtain a general solution for the effect of PP variation on the matrix deformation, and thus a fully coupled solution for the general deformation of grains-fluid system, is via a granular dynamics algorithm [e.g., *McNamara et al.*, 2000; *El Shamy and Zeghal*, 2007; *Okada and Ochiai*, 2007]. The second reason to use the infinitely stiff approximation is that it may be solved analytically, and although it is a simple end-member, its solution already provides a wealth of behaviors that should be considered as the basis for understanding the fully coupled system.

[27] The infinite stiffness approximation assumes that local pore volume collapse and expansion arc externally prescribed and are characterized by $\nabla \cdot \mathbf{u_s} < 0$ in equation (10) or $\dot{\Phi} < 0$ in equation (12). These will lead to pore fluid pressurization and depressurization and to the generation of PP gradients. In a fully coupled formulation the pressure gradients will oppose the pore collapse deformation by exerting a force that will act to push the pore walls aside in the case of compaction and push the pore walls inward in the case of expansion. Thus, the PP gradients somewhat relax the source of pressurization. For that reason the maximum PP within a fully coupled system is limited by the order of magnitude of the confining stress that drives pore volume change. In that sense the magnitude of the PP achieved under the infinite stiffness approximation serves as an upper bound with respect to a fully coupled system.

4.1. Application to Shearing of Fluid-Filled Uniform Granular System

[28] Here we explore the physical behavior of equation (10) under poroplastic conditions. This exploration is a first step in mapping the conditions that will cause liquefaction by irreversible pore volume collapse during shear of a granular system. For that, a simple system of hexagonally packed uniform grains immersed in fluid is studied (Figure 2). Packed uniform grains were previously considered theoretically [e.g., *Rowe*, 1962; *Iverson*, 1993], experimentally [e.g., *Iverson and Lahusen*, 1989; *Frye and Marone*, 2002], and

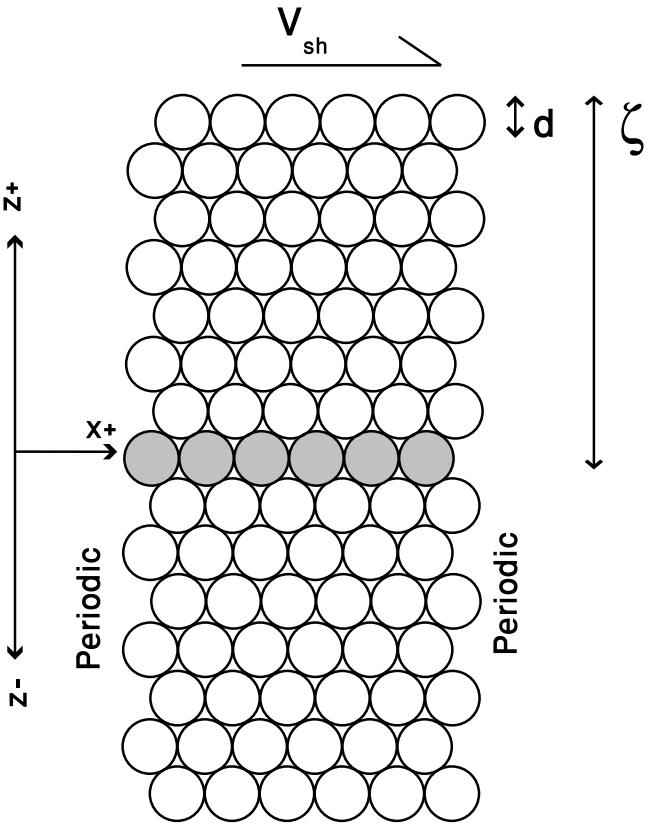

Figure 2. Model geometry for section 4.1. A hexagonal packing of fluid-filled granular material is being subjected to a constant shear velocity, V_{sh}. Shear displacement is accommodated along a single row marked by the grey grains. The boundaries along the x direction are periodic, and therefore, $\partial \mathbf{u_{sx}}/\partial x = 0$; d is a grain diameter, ζ is the distance to the boundaries, and 2ζ is system thickness.

numerically [*Makedonska et al.*, 2010]. In the system we consider here, the top boundary is sheared at a constant shear velocity, V_{sh}, in the $+x$ direction. The system is assumed to respond by localized shear deformation along one row of grains (Figure 3a, sliding row in grey). Along the x direction the system is assumed periodic and hence the divergence of the velocity in equation (10) is reduced to $\nabla \cdot \mathbf{u_s} = \partial \mathbf{u_{sz}}/\partial z$, where $\mathbf{u_{sz}}$ is the z component of the solid grains velocity, and the problem becomes one dimensional. The porosity, Φ, and the granular velocity perpendicular to the shear direction, $\mathbf{u_{sz}}$, of the sliding row of grains are functions of time, t (and thus of displacement, x):

$$\begin{aligned} \mathbf{u_{sz}} &= V_{sh}\frac{[\cos(\pi/3) - V_{sh}t'/d]}{A} \\ \Phi &= 1 - \frac{\pi}{4A} \\ A &= \sqrt{1 - [\cos(\pi/3) - V_{sh}t'/d]^2}. \end{aligned} \tag{15}$$

where $t' = (t + x'/V_{sh}) \bmod (d/V_{sh})$, and $0 \le x' \le d$ depends on the initial conditions as explained below. The simulated domain of thickness 2ζ is assumed to be buried at depth h (where $2\zeta \le h$), so that excess PP of $P = \sigma_d$ is interpreted as resulting in zero effective stress and the onset of liquefaction. The shearing row is located at distance ζ from the boundaries of the system.

[29] In the simulations, we aim to study the influence of the drainage boundary conditions on the evolution of PP. For that, there is a need to define an additional Deborah number, $\mathrm{De}_\zeta = t_\zeta/t_0$, termed the system Deborah number. De_ζ expresses the ratio between $t_\zeta = \zeta^2/D$, the timescale of PP diffusion over the system half thickness, and t_0, the timescale of deformation. When $\mathrm{De}_\zeta \ll 1$, PP can easily diffuse from the shearing row to the boundaries in the timescale of deformation, and as a result the PP along the shearing row feels the drainage conditions on the boundaries. When $\mathrm{De}_\zeta \gg 1$, the PP diffusion front originating along the shearing row does not reach the boundaries in the timescale of deformation. Therefore, the PP along the shearing row is indifferent to the drainage conditions along the boundaries.

[30] Three scenarios are tested. In the first two cases ζ is relatively small and therefore $\mathrm{De}_\zeta \ll 1$: In a *drained* system, a constant PP of $P = 0$ is assumed at the top of the system, as if an open fracture drains the buried domain at its top. In an *undrained* system, zero fluid flux across the top boundary is assumed, simulating an impermeable layer that lies on top of the domain. In these two cases the bottom boundary is assumed undrained. In the third case, ζ is relatively large resulting in $\mathrm{De}_\zeta \gg 1$. In this case the prescribed boundary conditions have no effect of the evolution of PP within the shearing row. The third case is termed *boundary-independent*. Table 1 summarizes the parameters used in the simulations.

[31] Two types of initial conditions are studied: In the first, denoted here as *dense packing*, the sliding row is initially in a hexagonal configuration (Figure 3a, sliding row in grey), and $x' = 0$. In this case, sliding is accompanied by initial dilation until a cubic configuration is reached along the sliding row. Then, the system compacts until hexagonal packing is reached again. A full period is the duration between two consecutive hexagonal configurations. In the second initial condition, termed here *loose packing*, the sliding row is initially placed in a cubic configuration with respect to the row below it (Figure 4a), and $x' = 0.5d$. In this case, the system first compacts to a full hexagonal configuration and then dilation along the sliding row brings it back to a cubic configuration. Here a full period is the duration between two consecutive cubic configurations.

[32] The set of equations (10) and (15) together with Carman-Kozeny equation (Table 1) for the relation between porosity and permeability are solved numerically using a 1D Crank-Nicholson scheme.

4.1.1. Dense Initial Packing

[33] First, the case of dense initial grain packing is studied; that is, all rows are initially hexagonally packed.

4.1.1.1. Drained

[34] Simulation results show that when the system is drained, the excess PP, initially taken as zero, becomes negative when the system starts to dilate as it shears (Figure 3b, red curve). As deformation continues, fluid influx from the top boundary, driven by the pressure gradient that forms between the top of the domain and the location of deformation, decreases the magnitude of this negative value. When a cubic configuration is reached; that is, the system has slid to its maximal porosity, PP is zero again. During compac-

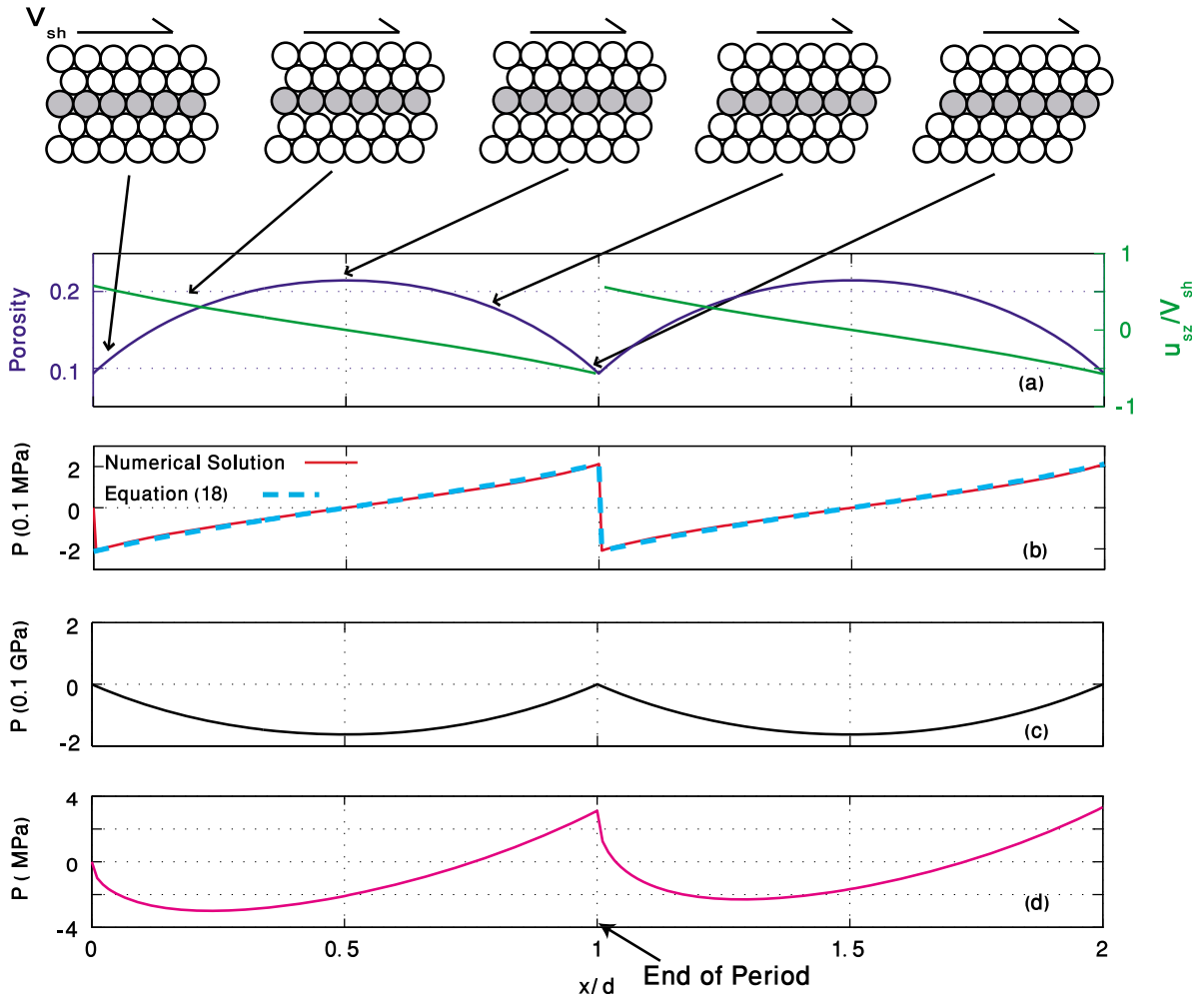

Figure 3. Simulation results of shearing of initially densely packed fluid-filled granular material at a constant shear velocity, V_{sh}, with parameters from Table 1. Shear is accommodated in a localized manner along a single sliding row, depicted by grey filled discs. The system first dilates to a cubic packing and then compacts back to a hexagonal packing. Dilation and compaction induce time and space dependent porosity, permeability and granular velocity. (a) Evolution of porosity (blue) and $\mathbf{u_{sz}}/V_{sh}$ (green) along the sliding row as a function of the horizontal displacement, x, scaled by grain diameter, d. (b) PP evolution along the sliding row, when the top boundary is drained. Maximum PP of 0.21 MPa is attained at the end of the period and corresponds to zero effective stress at depth of around 14 m. Red curve is the simulation results and turquoise dashed curve is an analytical prediction following equation (18). (c) PP evolution along the sliding row when the top boundary is undrained, showing that PP becomes increasingly negative when the system dilates and then returns to zero upon compaction. (d) PP evolution along the sliding row when $\mathrm{De}_\zeta \gg 1$ (boundary-independent). A combination of the two previous regimes is observed with maximum positive PP of 3.3 MPa at the end of the second period.

tion, PP rises until it gets to its maximal value when the system is back in hexagonal packing.

4.1.1.2. Undrained

[35] For an undrained system, the excess PP becomes increasingly negative during dilation and returns to zero when the system compacts again (Figure 3c). This occurs because during dilation the pore volume expands and $\nabla \cdot \mathbf{u_s} > 0$. With no fluid supply from the boundaries, the average PP must decrease. During compaction $\nabla \cdot \mathbf{u_s} < 0$, and PP increases back to the initial zero value. Since PP is negative throughout this simulation, overpressure is not generated. In fact the opposite is true as fluid becomes underpressured.

4.1.1.3. Boundary Independent

[36] The third scenario, of a large system with $\mathrm{De}_\zeta \gg 1$, shows PP evolution that is a combination of the drained and the undrained regimes (Figure 3d). Initially, the PP evolves similarly to an undrained system. However, the effect of fluid flow oriented toward the shearing row compensates for the negative value, so that minimum PP is attained before cubic packing, and PP increases to positive value at the end of the period similar to a drained system.

4.1.2. Loose Initial Packing

[37] Next, initially loose (cubic) packing systems are sheared. During the first half of the period, for all boundary

Table 1. Model Parameters for Section 4.1

Symbol		Value
β	Water compressibility	4.5×10^{-10} Pa^{-1}
μ	Water viscosity	10^{-3} Pa s
d	Grain diameter	5×10^{-4} m
2ζ	Layer thickness for drained and undrained	0.01 m
	Layer thickness for boundary-independent	4 m
V_{sh}	Shearing velocity	0.1 m/s
$\Phi_{\min}$	Porosity of hexagonal packing	0.093
k	Permeability (Carman-Kozeny)	$d^2\Phi^3/180(1-\Phi)^2$ m^2
D	Diffusion coefficient	$D_c = k_{\min}/\beta\mu\Phi_{\min} = 32.45$ m^2/s
l_k	PP diffusion length scale	$\sqrt{D_c t_0} = 0.4$ m[a]
De_d	Grain Deborah number	$t_d/t_0 = 1.54 \times 10^{-6}$[a]
De_ζ	System Deborah number for drained and undrained	$t_\zeta/t_0 = 1.54 \times 10^{-4}$[a]
	System Deborah number for boundary-independent	$t_\zeta/t_0 = 24.7$[a]

[a]Calculated with D_c.

conditions, the system compacts and PP increases. Maximum values are attained in the middle of the period when the systems are in hexagonal configuration (Figure 4). We next review the systems behavior during the second half of the period, when they dilate back to cubic packing.

4.1.2.1. Drained

[38] When a drained system starts dilating in the second half of the period, PP first drops to a negative value and then rises back to zero due to fluid influx from the boundary (Figure 4b).

4.1.2.2. Undrained

[39] For the undrained system, in the second half of the period, when dilation starts, PP returns to zero from its maximal value (Figure 4c, black curve). Here, excess PP is positive throughout the simulation.

4.1.2.3. Boundary Independent

[40] Simulations of a large system with $\mathrm{De}_\zeta \gg 1$ shows that in the second half of the period, upon dilation, PP decreases to a negative value, but the period ends with an increasing trend (Figure 4d). The overall evolution of PP is a combination of the drained and the undrained regimes, with minimum PP occurring not immediately upon initiation of dilation, like in a drained system and not at the end of the period like in an undrained system, but somewhere in between.

4.1.3. Results

[41] We have performed six simulations with two different initial conditions (loose and compacted), two system sizes, and two boundary conditions (drained and undrained). Several insights arise. When an undrained layer with $\mathrm{De}_\zeta \ll 1$ is sheared, then only negative PP is generated when the packing of grains is initially dense. But when the packing is initially loose pore fluid is pressurized and reaches 0.16 GPa, a value corresponding to σ_d at depth of 10 km, or alternatively, a value that reduces the effective stress along gouge material buried at depth of 15 km by more than 70%. It should be remembered that under the infinite stiffness approximation used here, the value of PP is not limited, and it is simply a function of the matrix deformation. In this framework, soil liquefaction at shallower depth is expected to take place early in the period. For example, reaching $P = \sigma_d$ at a depth of 10 m requires the generation of excess PP of 0.15 MPa, which occurs after 1% of a period ($t = 0.01d/V_{sh}$). When the infinite stiffness assumption is relaxed, the value of maximum PP is expected to be bounded by the order of magnitude of the confining stress, because PP gradients between the system interior and exterior will act to oppose further pore volume compaction and limit pressurization to the exact value that dynamically balances the forces acting to compact pore volume.

[42] In contrast, when some drainage exists pore fluid pressurization (to positive values) occurs even when the granular matrix is initially dense (or over-consolidated, as is called in soil mechanics), since shear involves first dilation and then compaction. For the completely drained system, with $\mathrm{De}_\zeta \ll 1$, excess PP becomes positive simultaneously with the initiation of compaction, and reaches a maximum of 0.21 MPa (for Table 1 parameters) corresponding to the effective normal stress at depth of 14 m. When $\mathrm{De}_\zeta \gg 1$, the PP becomes positive after some delay from the onset of compaction, and reaches a maximum of 3.3 MPa (for dense packing), corresponding to the effective stress at depth of 220 m. In these cases pore fluid pressurization occurs even for initially dense systems as long as there is a compaction phase that follows the dilation.

5. Physics of the PP Equation

[43] In light of our simulation results, we turn to analyze the behavior of the PP equation (10) under different drainage regimes.

5.1. Drained Boundary Conditions

[44] When the boundaries are well drained, fluid may flow freely into or out of the system, and PP gradients should evolve between the layer interior and the boundaries. (Here the boundary is maintained at a constant PP). Moreover, since $\mathrm{De}_d \ll 1$, the non-dimensional equation (9) reveals that the diffusion term is large, and the first time dependent term may be neglected relative to it. The PP equation (10) may then be approximated as

$$\nabla \cdot [k(\mathbf{x},t)\nabla P(\mathbf{x},t)] = \mu \nabla \cdot \mathbf{u_s}(\mathbf{x},t). \tag{16}$$

This form of PP response under drained conditions agrees with a Biot-based formulation by *Iverson* [1993]. In the 1D case, equation (16) may be expressed as

$$\frac{\partial P(z,t)}{\partial z} = \frac{\mu}{k(z,t)}\mathbf{u_{sz}}(z,t) + C(t), \tag{17}$$

where $C(t)$ is an integration factor. Note that equations (16) and (17) are independent of the fluid compressibility, β.

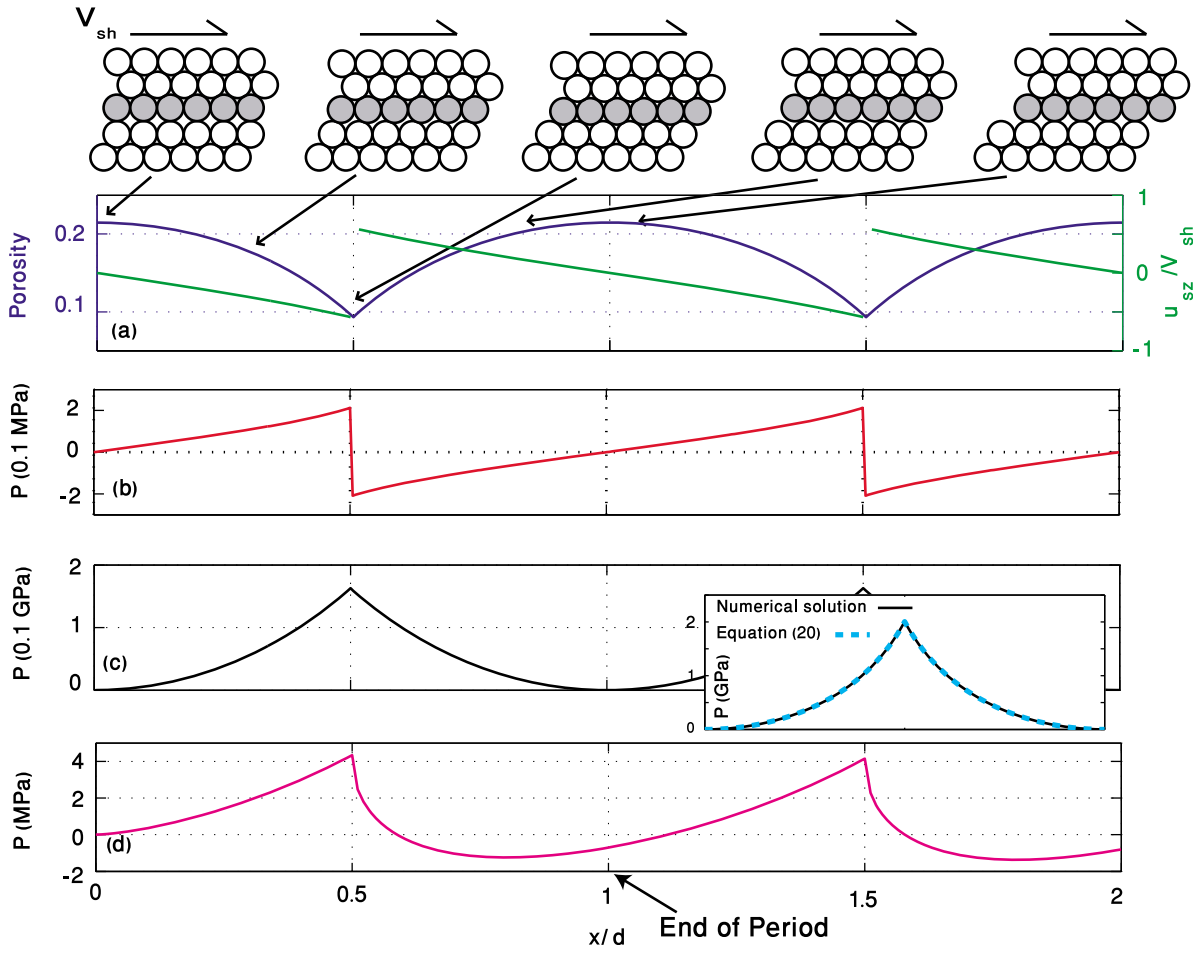

Figure 4. Simulation results of shearing of loosely packed fluid-filled granular material at a constant shear velocity, V_{sh}, with Table 1 parameters. Shear is accommodated in a localized manner along a single sliding row, depicted by grey filled discs. The system first compacts from a cubic configuration to a hexagonal configuration and then dilates back to cubic order. (a) Evolution of porosity (blue) and $\mathbf{u_{sz}}$ (green) along the sliding row as a function of the horizontal displacement, x, scaled by grain diameter, d. (b) PP along the sliding row that accommodates compaction and dilation with drained top evolves similarly to shearing of dense packing (Figure 3b), but with a shift of half period. (c) PP evolution along the sliding row with undrained top showing pore fluid pressurization with maximum of 0.16 GPa, corresponding to zero effective stress at a depth greater than 10 km, in the middle of the period. The inset shows simulation results (black curve) for PP evolution along the sliding row when the permeability is zero throughout the system to oppress PP diffusion, and analytical prediction (turquoise dashed curve) following equation (20) that assumes no diffusion. (d) PP evolution along the sliding row when $\mathrm{De}_\zeta \gg 1$, showing a combination of the two previous regimes.

This corresponds to a regime where the fluid may be considered as incompressible.

[45] The evolution of PP in our drained simulations (with $\mathrm{De}_\zeta \ll 1$) should follow equation (17). The pressure gradient may be estimated as $\partial P/\partial z = -P/\zeta$, and the PP along the sliding row is then approximated as

$$P = -\frac{\mu\zeta}{k}\mathbf{u_{sz}}. \tag{18}$$

The PP evolution according to equation (18) is compared to the numerical solution (Figure 3b, dashed turquoise curve). The parameters are taken from Table 1, and the permeability $k = k_{\min}$ is taken as the permeability resulting from the porosity of the hexagonal packing that is constantly preserved in the simulations, on top of the sliding row. Excluding the very onset of the motion that is governed by the time dependent term of equation (10), the analytical approximation, equation (18), and the numerical solution match.

[46] Equation (18) reveals that in the drained case the value of the PP along the shearing row depends linearly on the fluid viscosity, μ, the distance to drainage, ζ, and on the inverse of the permeability k^{-1}. For Carman-Kozeny law (Table 1), $k \propto d^2$, and thus $P \propto d^{-2}$. All these dependencies, together with fluid compressibility independency, were verified in a parametric sensitivity study.

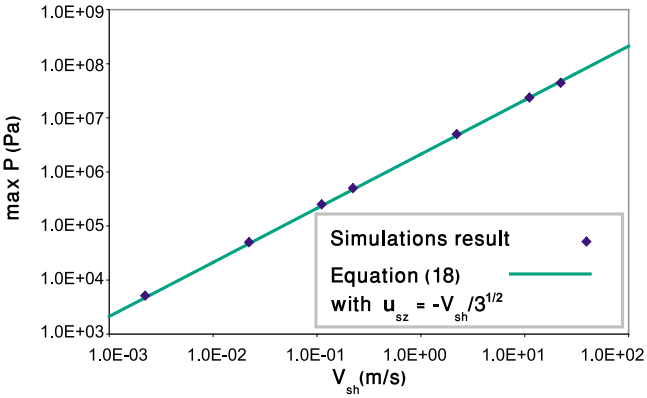

Figure 5. Simulation results with drained conditions (diamonds) for the relation between shear velocity V_{sh} and the maximum value of PP attained at the end of a shearing period. Analytical curve is based on equation (18) assuming $\mathbf{u_{sz}} = -V_{sh}/\sqrt{3}$ (see text), Table 1 parameters and permeability, $k_{\min}$, induced by hexagonal packing porosity (solid line). The slope of the linear relation between P and V_{sh} is a function of fluid viscosity, distance to drainage and inverse of permeability.

[47] Using equation (15), another dependency may be established: The maximum value for the PP, $P_{\max}$, is attained at the end of the period, when $t' = d/V_{sh}$. Assigning this value of t' in equation (15), it is found that $\mathbf{u_{sz}}$ $(t' = d/V_{sh}) = -V_{sh}/\sqrt{3}$. Using this $\mathbf{u_{sz}}$ in equation (18) predicts a linear relation between $P_{\max}$ and shear velocity, V_{sh}, as depicted in Figure 5.

5.2. Undrained Boundary Conditions

[48] When the boundaries are undrained, fluid cannot flow into or out of the granular layer, and fluid mass is conserved. Under such conditions, no pressure gradients arise across the boundaries. If the quantity of interest is the average value of PP within the layer, then the second diffusion term in equation (10) becomes zero (due to both averaging and zero pressure gradients on the boundaries). The average PP is then approximated as

$$P(t) = -\frac{1}{\beta}\int_0^t \frac{\nabla \cdot \mathbf{u_s}(t')}{\Phi(t')}\, dt', \tag{19}$$

where P depends on the fluid compressibility, β.

[49] The PP evolution in our undrained simulations is expected to follow equation (19). Evaluating $\nabla \cdot \mathbf{u}$ as $\mathbf{u_{sz}}/d$ and assigning the expressions for $\mathbf{u_{sz}}$ and Φ from equation (15):

$$P = -\frac{1}{\beta}\left\{\frac{\pi}{4}\ln\left[\frac{\pi - 4A}{\pi - 4}\right] + A - 1\right\}$$
$$A = \sqrt{1 - [\cos(\pi/3) - V_{sh}t'/d]^2}. \tag{20}$$

Comparison between equation (20) and the numerical solution assuming the PP does not diffuse away from the shearing row shows good fit (Figure 4c, inset). Equation (20) indicates that in the absence of PP diffusion, P is independent of the shearing velocity, V_{sh}, but is a function of the inverse fluid compressibility, β^{-1}. Small β will increase the PP.

5.3. Boundary Independent

[50] When the system Deborah number is large, $\mathrm{De}_\zeta \gg 1$, then the PP within the layer is indifferent to the type of imposed drainage boundary conditions. Since the boundaries are remote from the system interior, relatively mild pressure gradients are expected to arise, and none of the terms in equation (10) may be neglected. Here, the evolution of PP results from the competition between pressurization and depressurization induced by the time dependent term of equation (10) and fluid flow originating from the diffusion term of equation (10).

[51] Our large-system simulations should follow this case. It is possible to derive an analytic solution for the full equation (10), under the restrictions of equation (15), and assuming that the diffusion coefficient is constant with time, i.e., $D = D_c = k_{\min}/\beta\mu\Phi_{\min}$. Appendix B shows this derivation, and Figure 6 presents the comparison between the analytic solution and a boundary-independent simulation conducted with an imposed constant diffusion coefficient D_c along its shearing row. The analytic prediction reveals that the characteristic pressure scale for the evolving PP may be expressed as $d/\beta\sqrt{\pi D_c t_0}$. For the parameters of Table 1 this scale is ~1.5 MPa, which is the order of magnitude of PP that is found in Figure 6.

6. Discussion

[52] This section discusses the physics of PP evolution in response to granular matrix deformation as concluded from our theoretical analysis and our simulations. We also discuss the implications of this physics to numerical, experimental and natural systems. First, we consider the mechanisms that control PP evolution based on the formulation presented in section 2 and the analysis presented in section 5. The basic equations for the PP evolution, equations (10) and (12), predict two different physical mechanisms that compete in controlling the evolution of PP, but their relative contribution is determined by the parameters and boundary conditions of the system. The two mechanisms are PI, porosity-change-induced pressurization and depressurization, and FI, flow-induced pressurization and depressurization.

6.1. Pressurization Mechanisms

6.1.1. Mechanism PI

[53] Mechanism PI operates under undrained conditions. Here, pore fluid that cannot escape and is trapped within a shrinking pore volume is pressurized (Figure 7a), while pore fluid that is trapped in an expanding pore volume is depressurized. The evolution of the average PP will follow equation (19), and the magnitude of pressurization and depressurization is controlled by the fluid compressibility, and by the overall pore volume change, $\Delta\Phi$, that is expressed by $\int_0^t \nabla \cdot \mathbf{u_s}\ (\mathbf{x},\ t')dt'$ in equation (19). In that sense this mechanism holds memory of previous states of porosity.

6.1.2. Mechanism FI

[54] Mechanism FI operates under well-drained conditions, and is less intuitive. Because of mass conservation,

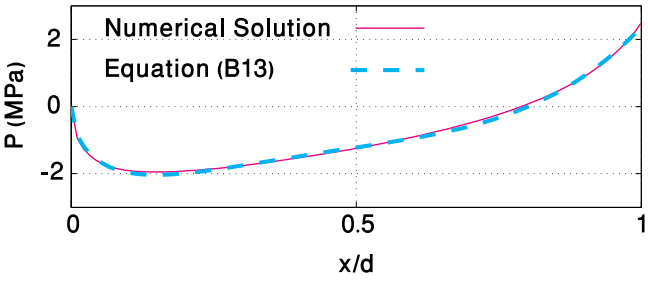

Figure 6. PP along the shearing row for large system with $De_\zeta \gg 1$, when the diffusion coefficient is assumed constant $D_c = k_{min}/\beta\mu\Phi_{min}$. Purple curve is simulation results, and the dashed turquoise curve is the analytic prediction following equation (B13).

convergence (or divergence) of grains causes the pore fluid that resides between the grains, to flow out of (or into) this region (Figure 7b). Because of fluid momentum conservation (here Darcy law), pressure gradients must arise between the location of converging (or diverging) grains and the surrounding, to generate these flows. Here, PP evolves from the arising pressure gradients, and is governed by equations (16) and (17). The magnitude of the generated pressure gradient depends on the rate of grains convergence or divergence, as expressed by $\nabla \cdot \mathbf{u_s}$ in equation (16). This mechanism holds no memory of previous states of porosity but pressurization depends on the instantaneous rate of pore deformation. Although it is not commonly considered as a mechanism for liquefaction, flow-induced PP evolution may lead to significant pressurization with PP that becomes high enough to fully support the normal stress [*Iverson and Lahusen*, 1989]. Moreover, because of its 'lack of memory', this mechanism may lead to generation of high PP even when an initially dense granular matrix is sheared. Indeed, upon shearing an over-compacted layer, it will first dilate (Figure 7b, left to center), and then oscillate around its critical porosity [*Aharonov and Sparks*, 2002; *Gabet and Mudd*, 2006]. In the oscillatory stage, any compaction phase, with $\nabla \cdot \mathbf{u_s} < 0$, will lead to pressurization despite the fact that the instantaneous

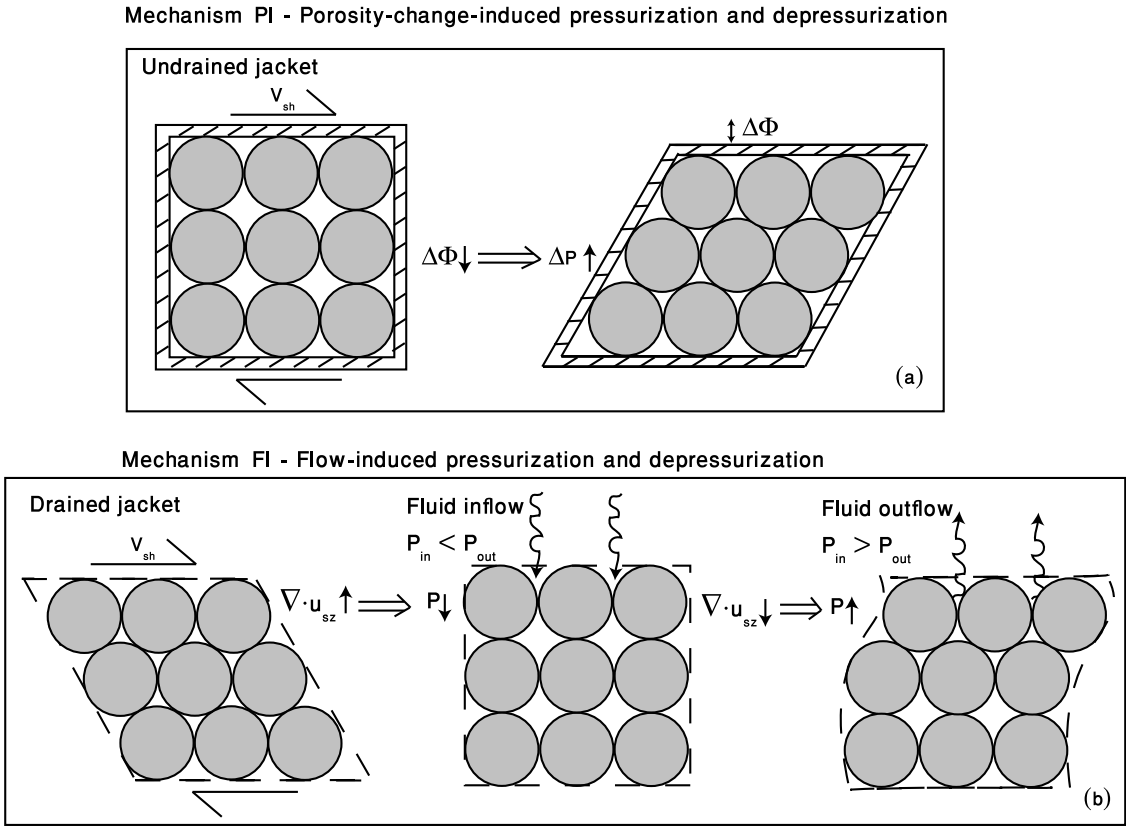

Figure 7. Two mechanisms control the evolution of PP in equation (10). (a) When fluid is trapped within a deforming pore volume (here, due to the undrained boundaries marked by double solid lines), any change of pore volume will cause the PP to evolve following mechanism PI. Compaction will lead to pressurization, and dilation will lead to depressurization. The magnitude of PP change depends on the overall change of porosity and on the inverse of fluid compressibility. (b) When fluid may flow freely in response to matrix deformation, (here, due to the well drained boundaries marked by dashed lines), PP evolution results from fluid flow following mechanism FI. Pressurization is a function of the instantaneous rate of matrix deformation. Upon dilation (left to center), fluid will flow into the system. In order to facilitate this flow, pressure gradient must arise with low pressure within the system interior. Upon compaction (center to right), fluid escapes from the system, and opposite PP gradient arises with higher PP in the system interior.

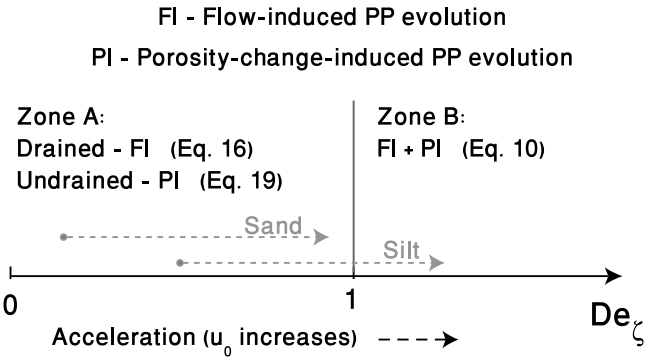

Figure 8. PP evolution mechanisms as a function of the system Deborah number, $De_\zeta = t_\zeta/t_0$, where t_ζ is the timescale of PP diffusion across the whole layer and t_0 is the timescale of deformation. When $De_\zeta \gg 1$ (zone B), both pressurization mechanisms operate simultaneously, like the case of boundary-independent simulations from section 4.1. When $De_\zeta \ll 1$ (zone A), the boundary conditions determine the PP evolution mechanism: Under undrained conditions, mechanism PI (porosity-change-induced) will dominate, and when the boundaries are drained, mechanism FI (flow-induced) will control the evolution of PP. The dashed grey lines show how the PP evolution mechanism changes during the acceleration of deformation in the nucleation stage of earthquakes. Upon acceleration De_ζ increases. Note that the starting points of the dashed lines are not to scale. See text for the evolution of sand and silt.

porosity may be significantly larger than the initial porosity (Figure 7b, center to right).

6.1.3. Relative Importance of Pressurization Mechanisms

[55] The relative importance of the two pressurization mechanisms for a specific system depends on both its properties and on its boundary conditions. These may have different characteristics, such as a strong contrast between internal and boundary permeabilities. The internal properties determine De_ζ, the system Deborah number, that expresses the ability of PP to diffuse across the whole layer in the timescale of deformation. When $De_\zeta \gg 1$ the drainage boundary conditions are not felt by the fluid within the system, and when $De_\zeta \ll 1$, drainage boundary conditions are well-felt by the pore fluid. For the boundary conditions, we consider here only the two end-members of completely drained boundaries that are connected to a constant pressure reservoir, and completely undrained boundaries that prevent fluid inflow and outflow. The exact combination of De_ζ, and boundary conditions determines which of the two PP evolution mechanisms will dominate.

[56] We present here a simple two-stage scheme that determines which mechanism for PP evolution will dominant, based on De_ζ, and the boundary conditions: (1) Evaluate De_ζ. If $De_\zeta \gg 1$, then both mechanisms of PP evolution, PI and FI, operate together (like the boundary-independent simulations that are tested in section 4.1), and there is no need to deal with the boundary conditions. If $De_\zeta \ll 1$, there is a need to move to the next stage. (2) Evaluate the drainage boundary conditions. If they are drained then the dominant mechanism is FI, flow-induced PP evolution. If they are undrained then mechanism PI will dominate. Figure 8 summarizes this scheme by presenting the dominant mechanism of PP evolution along a De_ζ axis.

[57] To illustrate the physics of these combinations, look at the last situation of $De_\zeta \ll 1$ (zone A in Figure 8), and undrained boundary conditions. In such a case, when the system undergoes compaction or dilation, pore fluid cannot flow away or into the system. However, PP can equilibrate within the system because PP can reach as far as the boundaries in the timescale of deformation. As a result, the evolution of the average PP will follow mechanism PI. Next in the discussion we apply this scheme to numerical, experimental, and natural systems.

6.2. Applications to Grains and Pore Fluid Modeling and Experiments

[58] When modeling a finite system of grains and fluid, the system parameters and boundary conditions are determined in advance. If the layer is thin, and PP diffusion can reach the boundaries in the timescale of deformation ($De_\zeta \ll 1$), but it is undrained, so that pore fluid cannot flow into or out of the layer, then mechanism PI, of pressurization by change of pore volume, will dominate. Therefore, fluid compressibility must be accounted for, but diffusive effects may be neglected, and the relevant equation to solve is (19). Pore fluid pressurization is expected only if the system is compacting with respect to its initial porosity, and the magnitude of PP is proportional to the inverse of fluid compressibility and to the amount of compaction.

[59] When modeling a thin drained layer, pore fluid can flow between the system interior and exterior. In order to facilitate this flow, pressure gradients arise between the system interior and the boundaries (assumed to be maintained at some constant pressure). The dominant PP evolution mechanism will be FI, flow-induced pressurization. Accounting for fluid compressibility will only introduce a short-lived transient effect, and if this effect is not of interest it is sufficient to solve Poisson equation (16). Pore fluid pressurization is expected when the system compacts with respect to any former state and not necessarily with respect to the initial state. Generated PP is linearly proportional to the compaction rate, fluid viscosity, distance to drainage, and the inverse of permeability.

[60] When the simulated layer is thick, and PP diffusion cannot reach the boundaries in the timescale of deformation, $De_\zeta \gg 1$ (boundary-independent), the drainage conditions along the boundaries do not affect the system dynamics and both pressurization mechanisms, PI and FI, operate simultaneously. In this case, both the diffusive term and the time dependent term with fluid compressibility should be accounted for, and the full fluid equation (10) should be solved (Figure 8).

[61] In light of these insights, we may now turn to analyze the two numerical models of *El Shamy and Zeghal* [2007] and *Okada and Ochiai* [2007] that are presented in section 1.1. *El Shamy and Zeghal* [2007] report the occurrence of liquefaction under drained conditions and with incompressible fluid. Such conditions are predicted to cause pressurization by mechanism FI due to pore fluid flow across the boundaries. *Okada and Ochiai* [2007] report the occur-

rence of liquefaction when compacting loose, undrained system, with compressible fluid. Such conditions lead to mechanism PI of PP evolution due to pore volume compaction. Thus, these two models simulate the two end-member mechanisms that are included in equation (10).

[62] Interpretation of experimental results should follow a similar scheme. *Samuelson et al.* [2009] performed a series of experiments, shearing fluid-filled granular material using a triaxial pressure vessel in a double direct shear configuration. We briefly revisit here their system, in order to demonstrate the applicability of our analysis to experiments. The parameters in the experimental system are $\zeta = 2 \times 10^{-3}$ m, $d = 1.27 \times 10^{-4}$ m, $u_0 = 10^{-6} - 10^{-4}$ m/s, $\Phi = 0.2$, and $k = 4.2 \times 10^{-14}$ m^2. PP was kept constant on the boundaries. This combination of parameters leads to a drained system, with $De_\zeta \ll 1$ (zone A in Figure 8). As a result, mechanism FI is expected to control PP evolution. Since *Samuelson et al.*'s [2009] experiments start with a well-compacted grain layer that dilates with shear, a transient negative PP leading to hardening is expected, similar to the effect observed in the beginning of our drained simulation (Figure 3b, red curve). However, with the parameters used in their experiments, this transient effect should last $< t_\zeta = 8.6 \times 10^{-6}$ s, while the sampling rate was 10^{-4} s. Therefore, it is expected that no dilatancy hardening will be observed. Indeed, *Samuelson et al.* [2009] report that "little if any dilatant hardening" occurs in their experiments.

6.3. Application to Natural Systems

[63] The formulation for the PP response to general granular matrix deformation, developed in section 2, is depth independent, and does not assume in advance the exact system properties and its boundary conditions. Therefore, it is next applied to analyze the mechanisms that control PP evolution in different field settings with granular layers that reside at various depths and are characterized by different boundary conditions: landslides' shear zones, fault gouge layers, and soils.

6.3.1. Liquefaction of Shear Zones

[64] As a first natural system we consider shear zones that accommodate large shear strain, similar to the uniform grain system that is studied in section 4.1. Critical state theory predicts, and experiments have shown, that during shear, loose soils contract while dense soils dilate [*Casagrande*, 1936]. In the past, it was suggested that liquefaction only occurs when loose granular material compacts, which lead to the conclusion that while loosely packed shear zones may liquefy due to grain collapse leading to PP rise, dense shear zones inhibit liquefaction as they do not allow pore fluid to be pressurized [*Iverson et al.*, 2000]. Indeed, here we find that if the shear zone of a landslide (with parameters similar to those studied in section 4.1) is confined by impermeable barriers, then the PP evolution within it will follow mechanism PI. In that case, only initially loose shear zones may become pressurized enough to facilitate mobilization of a landslide into a debris flow, as discussed by *Iverson et al.* [2000].

[65] However, in many cases, natural shear zones are initially highly compacted. It was observed that during shear motion at the base of landslides and also during earthquakes, the strain is large enough for the shear zone to dilate, and reach its critical porosity [*Iverson*, 2005]. That is, an over-compacted shear zone will first dilate, and then after the first several centimeters to several meters of displacement [*Iverson*, 2005; *Garagash and Rudnicki*, 2003] its porosity will oscillate around some steady state value. Such oscillations include also compacting phases, not with respect to the initial over-compacted configuration, but with respect to the critical porosity. If the shear zone is well drained, then mechanism FI, of flow-induced pressurization, may operate, causing significant PP increase during compaction phrases, and potentially leading to liquefaction and acceleration of shear.

[66] *Gabet and Mudd* [2006] report on debris flows mobilization from initially dense soils, and claim that this observation is not well understood since "it is generally accepted that liquefaction only occurs in soils that have porosity greater than the critical-state porosity" [*Gabet and Mudd*, 2006, p. 213], i.e., by mechanism PI. Following their observation, *Gabet and Mudd* [2006] reviewed the possibility that initially dense landslides first slide a limited distance, being arrested by PP reduction due to dilation, but then PP is rebuilt and triggers a second sliding phase, this time from an initially loose configuration. The second phase leads to liquefaction and to debris flow mobilization. *Gabet and Mudd* [2006] further find a correlation between debris flow mobilization and fines/sand ratio. They suggest that soils with a small ratio are mobilized due to their high hydraulic conductivities allowing for rapid fluid inflow and PP rise that leads to the second sliding phase. Following the analysis presented here, it is suggested that initially dense well-drained soils suck in pore fluid during dilation, thus allowing PP rise by mechanism FI during any short compactive stage that follows the initial dilative phase. Mechanism FI may then be responsible for mobilization of debris flow in initially dense shear zones, formulating a continuous version of the mechanics proposed by *Gabet and Mudd* [2006].

6.3.2. Soil Liquefaction

[67] Next we address the mechanism of PP evolution during soil liquefaction. The classical view of soil liquefaction attributes the rise of PP to cyclic strain of the soil skeleton [*Sawicki and Mierczynski*, 2006]. The formulation developed in section 2 is general and does not assume specific forcing, but the analysis of shearing uniform grain system presented in section 4.1 is built upon continuous shearing. We claim here that if the cyclic strain is large enough to allow both dilation and compaction of a single grain layer (shear deformation $\geq$ grain radius), then the behavior observed for continuous shearing is analogous to cyclic shearing. Still, positive PP may evolve only if the soil experiences some compaction during its deformation, but the feasibility and magnitude of compaction depend strongly on the initial porosity and on the duration of the applied force, that are beyond the scope of this paper. Here we discuss the mechanisms by which PP may evolve given an optimal deformation of the soil skeleton.

[68] We start by analyzing the conditions and mechanisms for soil liquefaction induced by the passage of seismic shear waves. We account for pore water and use water compressibility and viscosity from Table 1. The porosity is taken to be $\Phi = 0.46$, which corresponds to medium void ratio for 3D packing of spheres [*Okada and Ochiai*, 2007]. We analyze the situations of medium sand and of silt with grain diameter of $d = 5 \times 10^{-4}$ and 5×10^{-5} m, respectively, and

corresponding permeabilities of $k = 10^{-10}$ and 10^{-14} m^2. These permeabilities are smaller than predicted by Carman-Kozeny (in particular for the silt) as it is assumed that grain size is not completely uniform. The velocity of deformation is taken to be the peak ground velocity (PGV) induced by the seismic waves. We use $u_0 = 0.1$ m/s, which is estimated to be the minimal PGV to induce liquefaction [*Kostadinov and Towhata*, 2002]. We further assume that the source of liquefaction lies at a depth of 5 m, and this is also the distance to the drained boundary, $\zeta = 5$. For these parameters, the system Deborah number is $De_\zeta = 10.34$ for the sand, and $De_\zeta = 1.034 \times 10^4$ for the silt, so that for both soil types $De_\zeta > 1$, and PP cannot reach the boundaries in the timescale of deformation. Following the scheme presented above, both mechanisms of PP evolution, PI and FI, should be considered (zone B in Figure 8).

[69] Larger permeability and smaller PGV will lead to smaller De_ζ, and may potentially lead to PP evolution by mechanism FI. However, such conditions are also expected to decrease the magnitude of the evolving PP, because in accordance with equation (18), the PP depends linearly on the PGV, and inversely on the permeability. For example, if the permeability of the medium sand is as large as $k = 10^{-9}$ m^2, and the PGV is $u_0 = 0.01$ m/s, then $De_\zeta = 0.1034$. In such a case only mechanism FI of flow-induced pressurization will be of importance. However, the maximum PP, according to equation (18) is 0.05 MPa, while the excess PP needed for liquefaction at depth of 5 m is 0.075 MPa.

[70] This simple analysis shows that the process of soil liquefaction should be evaluated via an outline similar to the boundary-independent system and that both mechanisms of PP evolution, FI and PI, are predicted to operate together. Because mechanism FI contributes to the evolution of PP, we predict that positive PP may evolve even if the soil is not strictly compactive, as long as some transient compaction occurs, similar to the case studied in Figure 4d. A possible documented example of such a scenario comes from the liquefaction event in Kobe, Japan, that followed the 1995 Great Hanshin Earthquake (M = 6.9). *Soga* [1998] reviewed the damage in the port facilities that were built on reclaimed island. It was found that soils that were vibro-compacted, and therefore are not expected to be compactive, were still liquefied.

6.3.3. Sliding Nucleation along Faults

[71] Finally in the discussion we address the evolution of PP during the stage of sliding nucleation along fault zones. Many fault zone systems are characterized by strong permeability and configuration contrasts between the gouge material and the surrounding blocks, so that the gouge layer may be considered as the granular system while the surrounding blocks impose the drainage boundary conditions. We consider here a well-compacted gouge layer of thickness $2\zeta = 0.1$. During the nucleation stage the deformation velocity accelerates, and as a result the timescale of deformation, t_0, decreases. Since the pressurization mechanism depends on t_0, it may change during the nucleation stage. The dashed grey lines in Figure 8 present this change.

[72] At the initial stage of nucleation, assuming $u_0 = 10^{-5}$ m/s, $De_\zeta \ll 1$ for both the sand and the silt that were considered previously. Therefore, they are located in zone A of Figure 8, where the boundary conditions dictate the pressurization mechanism that will operate. If the confining blocks are impermeable, PP will evolve following mechanism PI according to changes of pore volume, and if the layer is initially over-compacted, negative excess PP will develop in response to any dilation, resulting in hardening. If the confining blocks are highly fractured and allow for communication with a fluid reservoir, then the PP will evolve following mechanism FI; that is, fluid inflow will compensate for the newly generated pore volume, and hardening will not occur [*Samuelson et al.*, 2009]. Upon acceleration, De_ζ increases, and when $u_0 = 0.1$ m/s, the sand remains in zone A, but the silt moves to zone B. Thus, the PP evolution within the silt gouge will become dependent on both mechanisms, FI and PI, regardless of the boundary conditions. Therefore, for small grain size, if the boundaries were previously drained and they remain so, and if dilation of the gouge continues during acceleration, some hardening is expected due to the fact that the systems moves from zone A to zone B in Figure 8, and mechanism PI starts to affect the system. This will introduce a force that acts to slow down the earthquake. If the boundaries were previously undrained and they become drained (e.g., by fracturing during sliding) then the initial negative PP will relax, but only after some delay.

7. Conclusions

[73] This paper presents a formulation describing pore fluid pressurization and flow in response to general granular matrix deformation, and is thus applicable to both elastic reversible deformation and to finite irreversible deformation. The formulation is used to examine the conditions and processes by which pore fluid pressure evolves to large enough values that may lead to liquefaction of soils and shear zones.

[74] It is found that the relative degree of drainage expressed by a Deborah number and by the boundary conditions is of great importance for the evolution of pore pressure (PP). There are two end-member mechanisms for PP evolution: FI, flow-induced pressurization and depressurization, and PI porosity-change-induced pressurization and depressurization. The first mechanism is newly offered, while the second mechanism was previously suggested to control PP evolution, though it was not completely understood. The system Deborah number, $De_\zeta = t_\zeta/t_0$, expresses the ratio between the timescale of relaxation by PP diffusion across the layer and the timescale of deformation. When $De_\zeta \ll 1$ then the type of boundary conditions determine which of the pressurization mechanisms operate. If the boundaries are undrained, PI dominates and pore fluid pressurization occurs only for initially loose granular matrices and is highly dependent on fluid compressibility, with faster pressurization for smaller compressibility. Under such conditions pressurization is not correlated to the rate of deformation but to the overall volumetric compaction. If the boundaries are drained, FI dominates and pore fluid pressurization occurs due to arising pressure gradients in response to pore fluid flow. In this pressurization mechanism PP may rise also in initially dense granular matrices during any later compaction stage that follows dilation. Here, PP depends on the compaction velocity, fluid viscosity, system permeability and distance to drainage, but is independent of fluid compressibility. This regime may explain liquefaction phenomena in initially dense and well drained soils and shear zones, conditions that were previously thought to be liquefaction resistant

despite field evidences showing otherwise [e.g., *Soga*, 1998; *Gabet and Mudd*, 2006]. When the system is large, or when deformation is rapid, $De_\zeta \gg 1$, and both fluid compressibility and the rate of deformation control the evolution of pore fluid pressure.

Appendix A: Comparison With Other Models

[75] Here, our equations (10) and (12) are compared to other models studying the response of PP to granular or porous matrix deformation. To facilitate comparison, the notation of this paper is adopted where possible.

A1. Elastic Formulations

[76] *Wang* [2000] presents two equivalent poroelastic formulations for the temporal and spatial evolution of PP in response to elastic forcing in a fluid-filled porous material. The first formulation describes the forcing as a temporal evolution of stress and is presented in equation (13). The second formulation describes the forcing in terms of temporal evolution of strain:

$$\frac{\partial P}{\partial t} = \frac{kM}{\mu}\frac{\partial^2 P}{\partial z^2} - \alpha M \frac{\partial \epsilon_{zz}}{\partial t}. \tag{A1}$$

Equation (A1) follows *Wang* [2000, equation (6.18)] with notation simplification following *Wang* [2000, equations (3.37) and (3.64)]. Where M is Biot's modulus and α is Biot-Willis coefficient. When grains are assumed incompressible, $M = 1/\beta\Phi$ and $\alpha = 1$ [*Wang*, 2000, Table 3.2]. Therefore equation (A1) may be rewritten as

$$\frac{\partial P}{\partial t} = \frac{k}{\mu\beta\Phi}\frac{\partial^2 P}{\partial z^2} - \frac{1}{\beta\Phi}\frac{\partial \epsilon_{zz}}{\partial t}. \tag{A2}$$

This form is equivalent to our equation (10), since the forcing term $\partial\epsilon_{zz}/\partial t$, representing the one dimensional strain rate, may be rewritten as $\partial \mathbf{u_{sz}}/\partial z$. For example, for a periodic strain of the form $\epsilon_{zz} = \epsilon_0 \exp(i\omega t)$, the corresponding grains velocity will be $\mathbf{u_{sz}} = \int_z (\partial\epsilon_{zz}/\partial t)dz = i\epsilon_0\omega z \exp(i\omega t)$. It is a surprising result that equation (A2) that was developed from a purely elastic point of view, is in fact equivalent to our equation (10), which did not assume elasticity. The only difference is *Wang*'s [2000] assumption of uniform permeability in the diffusion term (first term on the righthand side) of equation (A2), which does not necessarily hold for the general formulation of equation (10).

[77] *Bachrach et al.* [2001] present a study of the propagation of pressure waves in a poroelastic material induced by stress forcing using Biot's equations. Next, the equivalency between *Bachrach et al.*'s [2001] formulation and equation (13) (which follows *Wang*'s [2000] equation (6.14)) is demonstrated under the assumption of negligible inertia, an assumption that is discussed in the following. Combining *Bachrach et al.*'s [2001] equations (7) and (11) and neglecting inertial terms, it is found that

$$\frac{\partial P}{\partial t} = \frac{k}{\mu} 2D\left(1 - \alpha\frac{2\alpha D}{H}\right)\frac{\partial^2 P}{\partial z^2} - \frac{2\alpha D}{H}\frac{\partial \sigma}{\partial t}. \tag{A3}$$

As before, $\alpha = 1$, is the Biot-Willis coefficient for incompressible grains. $D = (2\beta\Phi)^{-1}$ and $H = K_\nu^{(u)} = K_\nu + (\beta\Phi)^{-1}$, where $K_\nu^{(u)}$ and K_ν are the undrained and drained uniaxial bulk moduli, respectively. H and D are resolved following their definition by *Bachrach et al.* [2001] and under the assumption of incompressible solid grains. Assigning the expressions for α, H and D into equation (A3) results in

$$\frac{\partial P}{\partial t} = \frac{k}{\mu}\frac{1}{\beta\Phi + K_\nu^{-1}}\frac{\partial^2 P}{\partial z^2} - \frac{1}{K_\nu^{(u)}\beta\Phi}\frac{\partial \sigma}{\partial t}. \tag{A4}$$

Following *Wang* [2000, equation (3.52)], $\beta\Phi + K_\nu^{-1} = S$, and following *Wang* [2000, equation (3.85) and Table 3.2], $(K_\nu^{(u)}\beta\Phi)^{-1} = \gamma$. Thus, it is shown that equation (A4) (which is an inertia free version of Biot's equations, as expressed in *Bachrach et al.*'s [2001] equations (7) and (11)) is identical to *Wang*'s [2000] equation (6.14) and to our equation (13).

[78] Next, we wish to determine the limits for the validity of our assumption of negligible inertia. For that, *Bachrach et al.*'s [2001] equations (7) and (11) are reviewed:

$$\begin{aligned} \rho_b\frac{\partial^2 v}{\partial t^2} + \rho_f\frac{\partial^2 w}{\partial t^2} &= \frac{\partial \sigma}{\partial z} \\ \rho_f\frac{\partial^2 v}{\partial t^2} + m\frac{\partial^2 w}{\partial t^2} &= \frac{\partial P}{\partial z} + \frac{\mu}{k}\frac{\partial w}{\partial t}, \end{aligned} \tag{A5}$$

where ρ_b is the density of the fluid-filled porous material, m is a coupling coefficient, and v and w are the displacement field of the solid matrix and fluid, respectively. Introducing scale factors for each of the variables: $v = w_0\hat{v}$, $w = w_0\hat{w}$, $\sigma = P_0\hat{\sigma}$, $P = P_0\hat{P}$, $z = L\hat{z}$, and $t = t_0\hat{t}$, where $t_0 = (2\pi f)^{-1}$, and f is the forcing frequency in s^{-1}. Assigning the scale factors in equation (A5), dropping the $\hat{}$ notation, and considering the magnitude of the densities ρ_f, ρ_b and the coupling coefficient, m, to be of the same order:

$$\begin{aligned} \frac{w_0\rho_f L(2\pi f)^2}{P_0}\left(\frac{\partial^2 v}{\partial t^2} + \frac{\partial^2 w}{\partial t^2}\right) &= \frac{\partial \sigma}{\partial z} \\ \frac{w_0\rho_f L(2\pi f)^2}{P_0}\left(\frac{\partial^2 v}{\partial t^2} + \frac{\partial^2 w}{\partial t^2}\right) &= \frac{\partial P}{\partial z} + \frac{\mu w_0 L(2\pi f)}{kP_0}\frac{\partial w}{\partial t}. \end{aligned} \tag{A6}$$

Taking $\rho_f = 10^3$ kg m^{-3}, $L = 1$ m, $P_0 = 100$ Pa, and $w_0 = 10^{-7}$ m following the values used by *Bachrach et al.* [2001], it is found that the acceleration terms, left-hand side of equation (A6), are important only for frequencies of an order ≥100 Hz, and may be neglected for smaller frequencies (a conclusion that also agrees with an analysis by *Iverson* [1993]). Thus, for smaller frequencies, *Bachrach et al.*'s [2001] formulation is equivalent to *Wang*'s [2000] equation (6.14) formulation, which by itself was shown to be similar to our equation (10).

A2. Non-Elastic Formulations

[79] *Walder and Nur* [1984] study processes of PP generation due to porosity reduction, accounting also for nonelastic deformation [*Walder and Nur*, 1984, equation (5)]:

$$\frac{\partial P}{\partial t} = \frac{k}{\mu\Phi(\beta + \beta_\Phi)}\nabla^2 P - \frac{1}{\Phi(\beta + \beta_\Phi)}\frac{\partial \Phi}{\partial t}_{irrev}. \tag{A7}$$

In this formulation, $\beta_\Phi = (1/\Phi)\,(\partial\Phi/\partial P)$ is the elastic pore compressibility, and $(\partial\Phi/\partial t)_{irrev}$ is the irreversible porosity evolution. With some algebraic transformation equation (A7) may be rewritten as

$$\frac{\partial P}{\partial t} = \frac{k}{\mu\Phi\beta}\nabla^2 P - \frac{1}{\Phi\beta}\left(\frac{\partial\Phi}{\partial t}_{rev} + \frac{\partial\Phi}{\partial t}_{irrev}\right), \tag{A8}$$

where the pore compressibility was expanded as $\beta_\Phi = (1/\Phi)\,(\partial\Phi/\partial t)_{rev}\,(\partial t/\partial P)$, and $(\partial\Phi/\partial t)_{rev}$ is the reversible component of the porosity change. Equation (A8) resembles our equation (12) under the assumption of space independent permeability. The forcing term of equation (A8) that is divided between reversible and irreversible porosity reduction is expressed as a single term in our equation (12). Therefore the forcing terms are identical up to a factor of $(1 - \Phi)$. This factor results from the different definitions of Darcy's velocity: *Walder and Nur* [1984] use $\mathbf{u_f} = -\frac{k}{\mu\Phi}\nabla P$ as if the matrix is stationary, while our formulation assumes that Darcy's velocity is given by equation (3).

[80] This appendix demonstrates that former formulation of PP generation by porous or granular matrix deformation may be reduced to our equations (10) or (12). That is, the formulations of *Wang* [2000], *Bachrach et al.* [2001], *Walder and Nur* [1984], and the formulations of *Snieder and van der Beukel* [2004] and *Samuelson et al.* [2009] that are not discussed here, all describe the temporal evolution of PP as a combination of a diffusion term and a forcing term.

Appendix B: Analytical Prediction for a Boundary-Independent System

[81] In this appendix we derive an analytical prediction for the temporal and spatial evolution of PP, for the model of fluid-filled uniform granular material, packed in hexagonal packing, under constant shear velocity, that is presented in section 4.1. This solution applies to the case of a large system with $\mathrm{De}_\zeta \gg 1$ (boundary-independent). The prediction is derived by solving equation (10) under the assumption of constant diffusion coefficient, $D_c = k_{\min}/\beta\mu\Phi_{\min}$, and using the evolution of granular velocity and porosity from equation (15). The equation to be solved is

$$\frac{\partial P}{\partial t} = D_c\frac{\partial^2 P}{\partial z^2} - \frac{1}{\beta}F(z,t), \tag{B1}$$

where $F(z, t)$ expresses the forcing $\nabla \cdot u_{sz}/\Phi$ that is concentrated along $z = 0$ (the shearing row), and is defined as

$$F(z,t) = \delta(z)V_{sh}\cdot u_F(t), \quad 0 < t < t_0 = d/V_{sh}, \tag{B2}$$

and

$$u_F(t) = \frac{u_{sz}}{\Phi} = \frac{(0.5 - t/t_0)}{\sqrt{1-(0.5-t/t_0)^2} - \pi/4}. \tag{B3}$$

$\delta(z)$ is Dirac delta function with units of m^{-1}, that stands for the $\nabla \cdot$ operator in equation (10). The solution of equation (B1) for $P(z, t)$ may be expressed using a Green's function by the integral [*McKenzie and Brune*, 1972]

$$P(z,t) = -\frac{1}{2\beta\sqrt{D_c\pi}}\int_0^t\int_{-\infty}^{\infty}\exp\left[-\frac{(z-z_i)^2}{4D(t-t_i)}\right]\frac{F(z_i,t_i)}{\sqrt{t-t_i}}dz_i dt_i. \tag{B4}$$

Assigning $F(z_i, t_i)$ from equation (B2), equation (B4) is evaluated as [*McKenzie and Brune*, 1972]

$$P(z,t) = -\frac{V_{sh}}{2\beta\sqrt{D\pi}}\int_0^t\exp\left[-\frac{z^2}{4D(t-t_i)}\right]\frac{u_F(t_i)}{\sqrt{t-t_i}}dt_i. \tag{B5}$$

To solve equation (B5), we first expand $u_F(t_i)$ as a third order power series of t_i using its third order interpolation polynomial, i.e., $u_F(t_i) = \sum_{j=0}^{j=3} a_j (t_i)^j$. In the next stage, $u_F(t_i)$ is rewritten as a third order power series of $(t - t_i)$, $u_F(t_i) = \sum_{j=0}^{j=3} b_j (t - t_i)^j$, where $b_j = b_j(t)$ is found by solving the system of linear equations:

$$\begin{aligned} b_0(t) &= a_0 + a_1 t + a_2 t^2 + a_3 t^3 \\ b_1(t) &= -a_1 - 2a_2 t - 3a_3 t^2 \\ b_2(t) &= a_2 + 3a_3 t \\ b_3(t) &= -a3, \end{aligned} \tag{B6}$$

and equation (B5) is rewritten as

$$P(z,t) = -\frac{V_{sh}}{2\beta\sqrt{D\pi}}\int_0^t\exp\left[-\frac{z^2}{4D(t-t_i)}\right]\frac{\sum_{j=0}^{j=3} b_j (t-t_i)^j}{\sqrt{t-t_i}}dt_i. \tag{B7}$$

Next, the following dimensionless variables are defined [*McKenzie and Brune*, 1972]:

$$\begin{aligned} \hat{P} &= \frac{\beta\sqrt{\pi D d/V_{sh}}}{d}P \\ \hat{t}_i &= t_i/t_0 \\ \hat{t} &= t/t_0 \\ \hat{z} &= \frac{1}{\sqrt{2D_c t_0}}z \end{aligned} \tag{B8}$$

and equation (B7) may be written in a non-dimensional form:

$$\begin{aligned} \hat{P}(\hat{z},\hat{t}) &= -\frac{1}{2}\int_0^{\hat{t}}\exp\left[-\frac{\hat{z}^2}{2(\hat{t}-\hat{t}_i)}\right]\frac{\sum_{j=0}^{j=3} b_j(\hat{t})(\hat{t}-\hat{t}_i)^j}{\sqrt{\hat{t}-\hat{t}_i}}d\hat{t}_i \\ &= -\left(b_0(\hat{t})\frac{1}{2}\int_0^{\hat{t}}\exp\left[-\frac{\hat{z}^2}{2(\hat{t}-\hat{t}_i)}\right]\frac{1}{\sqrt{\hat{t}-\hat{t}_i}}d\hat{t}_i\right) \\ &\quad -\left(b_1(\hat{t})\frac{1}{2}\int_0^{\hat{t}}\exp\left[-\frac{\hat{z}^2}{2(\hat{t}-\hat{t}_i)}\right]\frac{(\hat{t}-\hat{t}_i)}{\sqrt{\hat{t}-\hat{t}_i}}d\hat{t}_i\right) \\ &\quad -\left(b_2(\hat{t})\frac{1}{2}\int_0^{\hat{t}}\exp\left[-\frac{\hat{z}^2}{2(\hat{t}-\hat{t}_i)}\right]\frac{(\hat{t}-\hat{t}_i)^2}{\sqrt{\hat{t}-\hat{t}_i}}d\hat{t}_i\right) \\ &\quad -\left(b_3(\hat{t})\frac{1}{2}\int_0^{\hat{t}}\exp\left[-\frac{\hat{z}^2}{2(\hat{t}-\hat{t}_i)}\right]\frac{(\hat{t}-\hat{t}_i)^3}{\sqrt{\hat{t}-\hat{t}_i}}d\hat{t}_i\right) \\ &= -[b_0(\hat{t})I_0 + b_1(\hat{t})I_1 + b_2(\hat{t})I_2 + b_3(\hat{t})I_3], \end{aligned} \tag{B9}$$

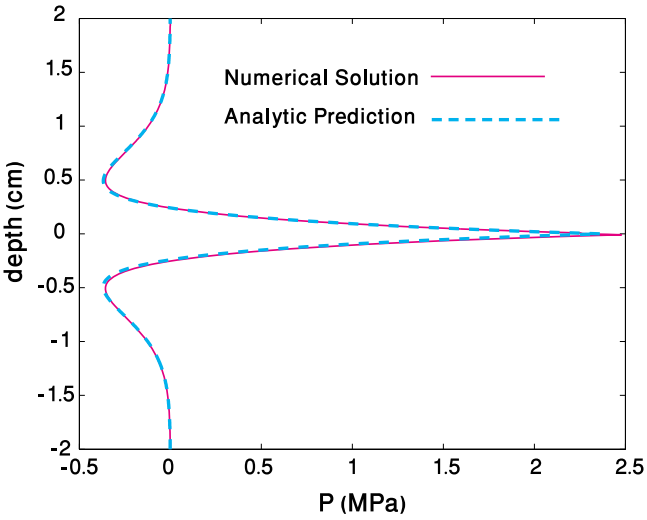

Figure B1. Spatial distribution of PP for a large system (with $De_\zeta \gg 1$) at the end of the period, $\hat{t} = 1$. The shearing row is in the middle of the domain. Purple curve is simulation results, and dashed turquoise curve is the analytical prediction for $P(z, d/V_{sh})$ following equations (B6)–(B12).

where I_i are the integrals. The solution for I_0 from *McKenzie and Brune* [1972] is

$$I_0 = \sqrt{\hat{t}}\exp\frac{-\hat{z}^2}{2\hat{t}} - \hat{z}\sqrt{\frac{\pi}{2}}\operatorname{erfc}\left(\frac{\hat{z}}{\sqrt{2\hat{t}}}\right). \tag{B10}$$

Integrals $I_1 - I_3$ can be integrated by parts and reduced to I_0 as follows:

$$\begin{aligned} I_1 &= \frac{1}{2}\int_0^{\hat{t}} \exp\left[-\frac{\hat{z}^2}{2(\hat{t}-\hat{t}_i)}\right]\frac{(\hat{t}-\hat{t}_i)}{\sqrt{\hat{t}-\hat{t}_i}}d\hat{t}_i \\ &= -\frac{1}{2}\int_{\hat{t}}^{0} \exp\left[-\frac{\hat{z}^2}{2\tau}\right]\tau^{1/2}d\tau \\ &= -\frac{1}{2}\left[\left(\frac{2}{3}\tau^{3/2}\exp\left[-\frac{\hat{z}^2}{2\tau}\right]\right)\Big|_{\hat{t}}^{0} - \frac{2}{3}\frac{\hat{z}^2}{2}\int_{\hat{t}}^{0}\exp\left[-\frac{\hat{z}^2}{2\tau}\right]\tau^{-1/2}d\tau\right] \\ &= \frac{1}{3}\left[\hat{t}^{3/2}\exp\left[-\frac{\hat{z}^2}{2\hat{t}}\right] - \hat{z}^2 I_0\right]. \end{aligned} \tag{B11}$$

Similarly, it can be shown that

$$\begin{aligned} I_2 &= \frac{1}{5}\left[\hat{t}^{5/2}\exp\left[-\frac{\hat{z}^2}{2\hat{t}}\right] - \hat{z}^2 I_1\right] \\ I_3 &= \frac{1}{7}\left[\hat{t}^{7/2}\exp\left[-\frac{\hat{z}^2}{2\hat{t}}\right] - \hat{z}^2 I_2\right]. \end{aligned} \tag{B12}$$

Equations (B6) and (B7)–(B12) give a full solution for $\hat{P}(\hat{z}, \hat{t})$. Evaluating $\hat{P}(\hat{z}, \hat{t})$ along the shearing row gives

$$\begin{aligned} P(0,\hat{t})\frac{\beta\sqrt{\pi D d/V_{sh}}}{d} = -\frac{1}{105}\sqrt{(\hat{t})}(582.929 - 1885.66\hat{t} \\ + 2667.73\hat{t}^2 - 1524.38\hat{t}^3) \end{aligned} \tag{B13}$$

where the coefficient of the interpolation polynomial for $u_F(\hat{t})$ are $a_0 = 5.5517$, $a_1 = -26.938$, $a_2 = 47.638$ and $a_3 = -31.758$. Figure 6 compares equation (B13) with boundary-independent simulation results conducted with a constant diffusion coefficient, D_c. Figure B1 compares the spatial pattern of PP at the end of the period ($\hat{t} = 1$) between boundary-independent simulations and the analytical prediction presented here.

[82] **Acknowledgments.** We thank Amotz Agnon and Michael Tsesarsky for fruitful discussions. We also wish to thank André Niemeijer, the Associate Editor, and an anonymous reviewer for constructive reviews that helped greatly in improving the manuscript.

References

Aharonov, E., and D. Sparks (2002), Shear profiles and localization in simulations of granular materials, *Phys. Rev. E*, *65*(5), 051302, doi:10.1103/PhysRevE.65.051302.

Anghel, D. V., M. Strauss, S. McNamara, E. G. Flekkøy, and K. J. Måløy (2006), Erratum: Grains and gas flow: Molecular dynamics with hydrodynamic interactions [Phys. Rev. E 61, 4054 (2000)], *Phys. Rev. E*, *74*(2), 029906, doi:10.1103/PhysRevE.74.029906.

Bachrach, R., A. Nur, and A. Agnon (2001), Liquefaction and dynamic poroelasticity in soft sediments, *J. Geophys. Res.*, *106*(B7), 13,515–13,526, doi:10.1029/2000JB900474.

Biot, M. A. (1941), General theory for three-dimensional consolidation, *J. Appl. Phys.*, *12*, 155, doi:10.1063/1.1712886.

Biot, M. A. (1956a), Theory of propagation of elastic waves in a fluid-saturated porous solid. I. Low-frequency range, *J. Acoust. Soc. Am.*, *28*, 168–178, doi:10.1121/1.1908239.

Biot, M. A. (1956b), Theory of propagation of elastic waves in a fluid-saturated porous solid. II. Higher frequency range, *J. Acoust. Soc. Am.*, *28*, 179–191, doi:10.1121/1.1908241.

Biot, M. A. (1962), Mechanics of deformation and acoustic propagation in porous dissipative media, *J. Appl. Phys.*, *33*(4), 1482–1498, doi:10.1063/1.1728759.

Blanpied, M. L., D. A. Lockner, and J. D. Byerlee (1992), An earthquake mechanism based on rapid sealing of faults, *Nature*, *358*(6387), 574–576, doi:10.1038/358574a0.

Casagrande, A. (1936), Characteristics of cohesionless soils affecting the stability of slopes and earth fills, *J. Boston Soc. Civ. Eng.*, *23*, 13–32.

Castro, G. (1969), *Liquefaction of Sands*, *Harvard Soil Mech. Ser.*, vol. 87, Harvard Univ., Cambridge, Mass.

Cetin, K. O., N. Isik, and B. Unutmaz (2004), Seismically induced landslide at Degirmendere Nose, Izmit bay during Kocaeli (Izmit)-Turkey earthquake, *Soil. Dyn. Earthquake Eng.*, *24*(3), 189–197, doi:10.1016/j.soildyn.2003.11.007.

Das, M. B. (1993), *Principles of Soil Mechanics*, PWS-Kent, Boston, Mass.

El Shamy, U., and M. Zeghal (2007), A micro-mechanical investigation of the dynamic response and liquefaction of saturated granular soils, *Soil. Dyn. Earthquake Eng.*, *27*(8), 712–729, doi:10.1016/j.soildyn.2006.12.010.

Flekkøy, E. G., A. Malthe-Sørenssen, and B. Jamtveit (2002), Modeling hydrofracture, *J. Geophys. Res.*, *107*(B8), 2151, doi:10.1029/2000JB000132.

Forterre, Y., and O. Pouliquen (2008), Flows of dense granular media, *Annu. Rev. Fluid Mech.*, *40*, 1–24, doi:10.1146/annurev.fluid.40.111406.102142.

Frye, K. M., and C. Marone (2002), The effect of particle dimensionality on granular friction in laboratory shear zones, *Geophys. Res. Lett.*, *29*(19), 1916, doi:10.1029/2002GL015709.

Gabet, E. J., and S. M. Mudd (2006), The mobilization of debris flows from shallow landslides, *Geomorphology*, *74*, 207–218, doi:10.1016/j.geomorph.2005.08.013.

Garagash, D. I., and J. W. Rudnicki (2003), Shear heating of a fluid-saturated slip-weakening dilatant fault zone: 1. Limiting regimes, *J. Geophys. Res.*, *108*(B2), 2121, doi:10.1029/2001JB001653.

Garga, V. K., and H. Zhang (1997), Volume changes in undrained triaxial tests on sands, *Can. Geotech. J.*, *34*, 762–772, doi:10.1139/cgj-34-5-762.

Hamiel, Y., V. Lyakhovsky, and A. Agnon (2005), Rock dilation, nonlinear deformation, and pore pressure change under shear, *Earth Planet. Sci. Lett.*, *237*(3–4), 577–589, doi:10.1016/j.epsl.2005.06.028.

Itasca Consulting Group, Inc. (2005), PFC3D (Particle Flow Code in 3 Dimensions), version 3.1., Minneapolis, Minn.

Iverson, R. M. (1993), Differential-equations governing slip-induced pore-pressure fluctuations in a water-saturated granular medium, *Math. Geol.*, *25*(8), 1027–1048, doi:10.1007/BF00911548.

Iverson, R. M. (2005), Regulation of landslide motion by dilatancy and pore pressure feedback, *J. Geophys. Res.*, *110*, F02015, doi:10.1029/2004JF000268.

Iverson, R. M., and R. G. LaHusen (1989), Dynamic pore-pressure fluctuations in rapidly shearing granular-materials, *Science*, *246*(4931), 796–799, doi:10.1126/science.246.4931.796.

Iverson, R. M., M. E. Reid, and R. G. LaHusen (1997), Debris-flow mobilization from landslides, *Annu. Rev. Earth Planet. Sci.*, *25*, 85–138, doi:10.1146/annurev.earth.25.1.85.

Iverson, R. M., M. E. Reid, N. R. Iverson, R. G. LaHusen, M. Logan, J. E. Mann, and D. L. Brien (2000), Acute sensitivity of landslide rates to initial soil porosity, *Science*, *290*(5491), 513–516, doi:10.1126/science.290.5491.513.

Johnsen, Ø., R. Toussaint, K. L. Måløy, and E. G. Flekkøy (2006), Pattern formation during air injection into granular materials confined in a circular Hele-Shaw cell, *Phys. Rev. E*, *74*(1), 011301, doi:10.1103/PhysRevE.74.011301.

Johnsen, Ø., R. Toussaint, K. J. Måløy, E. G. Flekkøy, and J. Schmittbuhl (2007), Coupled air/granular flow in a linear Hele-Shaw cell, *Phys. Rev. E*, *77*(1), 011301, doi:10.1103/PhysRevE.77.011301.

Johnsen, Ø., C. Chevalier, A. Lindner, R. Toussaint, E. C. K. J. Måløy, E. G. Flekkøy, and J. Schmittbuhl (2008), Decompaction and fluidization of a saturated and confined granular medium by injection of a viscous liquid or a gas, *Phys. Rev. E*, *78*(5), 051302, doi:10.1103/PhysRevE.78.051302.

Kawakami, F., and A. Asada (1966), Damage to the ground and earth structures by the Niigata earthquake of June 16,1964, *Soil Found.*, *6*(1), 14–30.

Kherbouche, R., J. F. Shao, F. Skoczylas, and J. P. Henry (1995), On the poroplastic behavior of porous rocks, *Eur. J. Mech. A, Solids*, *14*(4), 577–587.

Kostadinov, M. V., and I. Towhata (2002), Assessment of liquefaction-inducing peak ground velocity and frequency of horizontal ground shaking at onset of phenomenon, *Soil. Dyn. Earthquake Eng.*, *22*(4), 309–322, doi:10.1016/S0267-7261(02)00018-0.

Kozlov, V. G., A. A. Ivanova, and P. Evesque (1998), Sand behavior in a cavity with incompressible liquid under vertical vibrations, *Europhys. Lett.*, *42*(4), 413–418, doi:10.1209/epl/i1998-00264-2.

Kramer, S. L. (1996), *Geotechnical Earthquake Engineering*, Prentice Hall, Upper Saddle River, N. J.

Li, X., X. Chu, and D. Sheng (2007), A saturated discrete particle model and characteristic-based SPH method in granular materials, *Int. J. Numer. Methods Eng.*, *72*, 858–882, doi:10.1002/nme.2037.

Makedonska, N., L. Goren, D. Sparks, and E. Aharonov (2010), What controls the effective friction of shearing granular media?, in *Meso-Scale Shear Physics in Earthquake and Landslide Mechanics*, edited by Y. H. Hatzor, J. Sulem, and I. Vardoulakis, pp. 191–203, CRC Press, Boca Raton, Fla.

Manzari, M. T., K. Arulanandan, and R. F. Scott (1994), VELACS project: A summary of achievements, in *Proceedings From the Fifth U.S.-Japan Workshop on Earthquake Resistant Design of Lifeline Facilities and Countermeasures Against Liquefaction*, edited by T. D. O'Rourke and M. Hamada, *Tech. Rep. NCEER-940-0026*, pp. 389–404, Natl. Cent. for Earthquake Eng. Res., State Univ. of N. Y. Buffalo, Buffalo.

Marone, C., C. B. Raleigh, and C. H. Scholz (1990), Frictional behavior and constitutive modeling of simulated fault gouge, *J. Geophys. Res.*, *95*, 7007–7025, doi:10.1029/JB095iB05p07007.

McKenzie, D., and J. N. Brune (1972), Melting on fault planes during large earthquakes, *Geophys. J. R. Astron. Soc.*, *29*, 65–78.

McNamara, S., E. G. Flekkøy, and K. J. Måløy (2000), Grains and gas flow: Molecular dynamics with hydrodynamic interactions, *Phys. Rev. E*, *61*(4), 4054–4059, doi:10.1103/PhysRevE.61.4054.

Miller, S. A., and A. Nur (2000), Permeability as a toggle switch in fluid-controlled crustal processes, *Earth Planet. Sci. Lett.*, *183*, 133–146, doi:10.1016/S0012-821X(00)00263-6.

Moore, P. L., and N. R. Iverson (2002), Slow episodic shear of granular materials regulated by dilatant strengthening, *Geology*, *30*(9), 843–846, doi:10.1130/0091-7613(2002)030<0843:SESOGM>2.0.CO;2.

Mourgues, R., and P. Cobbold (2003), Some tectonic consequences of fluid overpressures and seepage forces as demonstrated by sandbox modelling, *Tectonophysics*, *376*(1–2), 75–97, doi:10.1016/S0040-1951(03)00348-2.

Okada, Y., and H. Ochiai (2007), Coupling pore-water pressure with distinct element method and steady state strengths in numerical triaxial tests under undrained conditions, *Landslides*, *4*, 357–369, doi:10.1007/s10346-007-0092-1.

Osswald, T. (1998), *Polymer Processing Fundamental*, Hanser Gardner, Cincinnati, Ohio.

Popescu, R., and J. H. Prevost (1995), Comparison between VELACS numerical class—A predictions and centrifuge experimental soil test-results, *Soil. Dyn. Earthquake Eng.*, *14*(2), 79–92, doi:10.1016/0267-7261(94)00038-I.

Rowe, P. W. (1962), The stress-dilatancy relation for static equilibrium of an assembly of particles in contact, *Proc. R. Soc. London, Ser. A*, *269*, 500–527, doi:10.1098/rspa.1962.0193.

Rozhko, A. Y., Y. Y. Podladchikov, and F. Renard (2007), Failure patterns caused by localized rise in pore-fluid overpressure and effective strength of rocks, *Geophys. Res. Lett.*, *34*, L22304, doi:10.1029/2007GL031696.

Saar, M. O., and M. Manga (2004), Depth dependence of permeability in the Oregon Cascades inferred from hydrologic, thermal, seismic and magnetic modeling constraints, *J. Geophys. Res.*, *109*, B04204, doi:10.1029/2003JB002855.

Samuelson, J., D. Elsworth, and C. Marone (2009), Shear-induced dilatancy of fluid-saturated faults: Experiment and theory, *J. Geophys. Res.*, *114*, B12404, doi:10.1029/2008JB006273.

Sawicki, A., and J. Mierczynski (2006), Developments in modeling liquefaction of granular soils, caused by cyclic loads, *Appl. Mech. Rev.*, *59*, 91–106, doi:10.1115/1.2130362.

Scawthorn, C., and P. I. Yanev (1995), Preliminary report 17 January 1995, Hyogo-ken Nambu, Japanese earthquake, *Eng. Struct.*, *17*(3), 146–157, doi:10.1016/0141-0296(95)00041-5.

Scholz, C. H. (1990), *The Mechanics of Earthquakes and Faulting*, Cambridge Univ, Press, Cambridge, U. K.

Segall, P., and J. R. Rice (1995), Dilatancy, compaction, and slip instability of fluid-infiltrated fault, *J. Geophys. Res.*, *100*(B11), 22,155–22,171, doi:10.1029/95JB02403.

Sidle, R. C., and H. Ochiai (2006), *Landslides Processes, Prediction, and Land Use*, *Water Resour. Monogr. Ser.*, vol. 18, AGU, Washington, D. C.

Skempton, A. W. (1960), Terzaghi's discovery of effective stress, in *From Theory to Practice in Soil Mechanics*, edited by L. Bjerrum et al., pp. 42–53, John Wiley, New York.

Sleep, N. H., and M. L. Blanpied (1992), Creep, compaction and the weak rheology of major faults, *Nature*, *359*(6397), 687–692, doi:10.1038/359687a0.

Snieder, A., and A. van der Beukel (2004), The liquefaction cycle and the role of drainage in liquefaction, *Granul. Matter*, *6*, 1–9, doi:10.1007/s10035-003-0151-9.

Soga, K. (1998), Soil liquefaction effects observed in the Kobe earthquake of 1995, *Proc. Inst. Civ. Eng. Geotech. Eng.*, *131*(1), 34–51, doi:10.1680/igeng.1998.30004.

Terzaghi, K. (1943), *Theoretical Soil Mechanics*, doi:10.1002/9780470172766, John Wiley, New York.

Vinningland, J. L., Ø. Johnsen, E. G. Flekkøy, R. Toussaint, and K. J. Måløy (2007a), Granular Rayleigh-Taylor instability: Experiments and simulations, *Phys. Rev. Lett.*, *99*(4), doi:10.1103/PhysRevLett.99.048001.

Vinningland, J. L., Ø. Johnsen, E. G. Flekkøy, R. Toussaint, and K. J. Måløy (2007b), Experiments and simulations of a gravitational granular flow instability, *Phys. Rev. E*, *76*(5), 051306, doi:10.1103/PhysRevE.76.051306.

Voight, B., and C. Faust (1982), Frictional heat and strength loss in some rapid landslides, *Geotechnique*, *32*(1), 43–54, doi:10.1680/geot.1982.32.1.43.

Walder, J., and A. Nur (1984), Porosity reduction and crustal pore pressure development, *J. Geophys. Res.*, *89*(B13), 11,539–11,548, doi:10.1029/JB089iB13p11539.

Wang, H. F. (2000), *Theory of Linear Poroelasticity With Applications to Geomechanics and Hydrogeology*, Princeton Univ. Press, Princeton, N. J.

Yamashita, T. (1999), Pore creation due to fault slip in a fluid-permeated fault zone and its effect on seismicity: Generation mechanism of earthquake swarm, *Pure Appl. Geophys.*, *155*, 625–647, doi:10.1007/s000240050280.

Youd, T. L. (1972), Compaction of sands by repeated shear straining, *J. Soil Mech. Found. Design*, *98*, 709–725.

Zienkiewicz, O. C., A. H. C. Chan, M. Pastor, B. A. Schrefler, and T. Shiomi (1999), *Computational Geomechanics With Special Reference to Earthquake Engineering*, John Wiley, Chichester, U. K.

E. Aharonov, Institute of Earth Sciences, Hebrew University, Givat Ram, Jerusalem 91904, Israel. (einatah@cc.huji.ac.il)

L. Goren, Department of Environmental Sciences and Energy Research, Weizmann Institute of Science, Rehovot 76100, Israel. (liran.goren@weizmann.ac.il)

D. W. Sparks, Department of Geology and Geophysics, Texas A&M University, College Station, TX 77843-3115, USA. (sparks@geo.tamu.edu)

R. Toussaint, IPGS, CNRS and University of Strasbourg, EOST, 5 rue René Descartes, F-67000 Strasbourg CEDEX, France. (renaud.toussaint@eost.u-strasbg.fr)